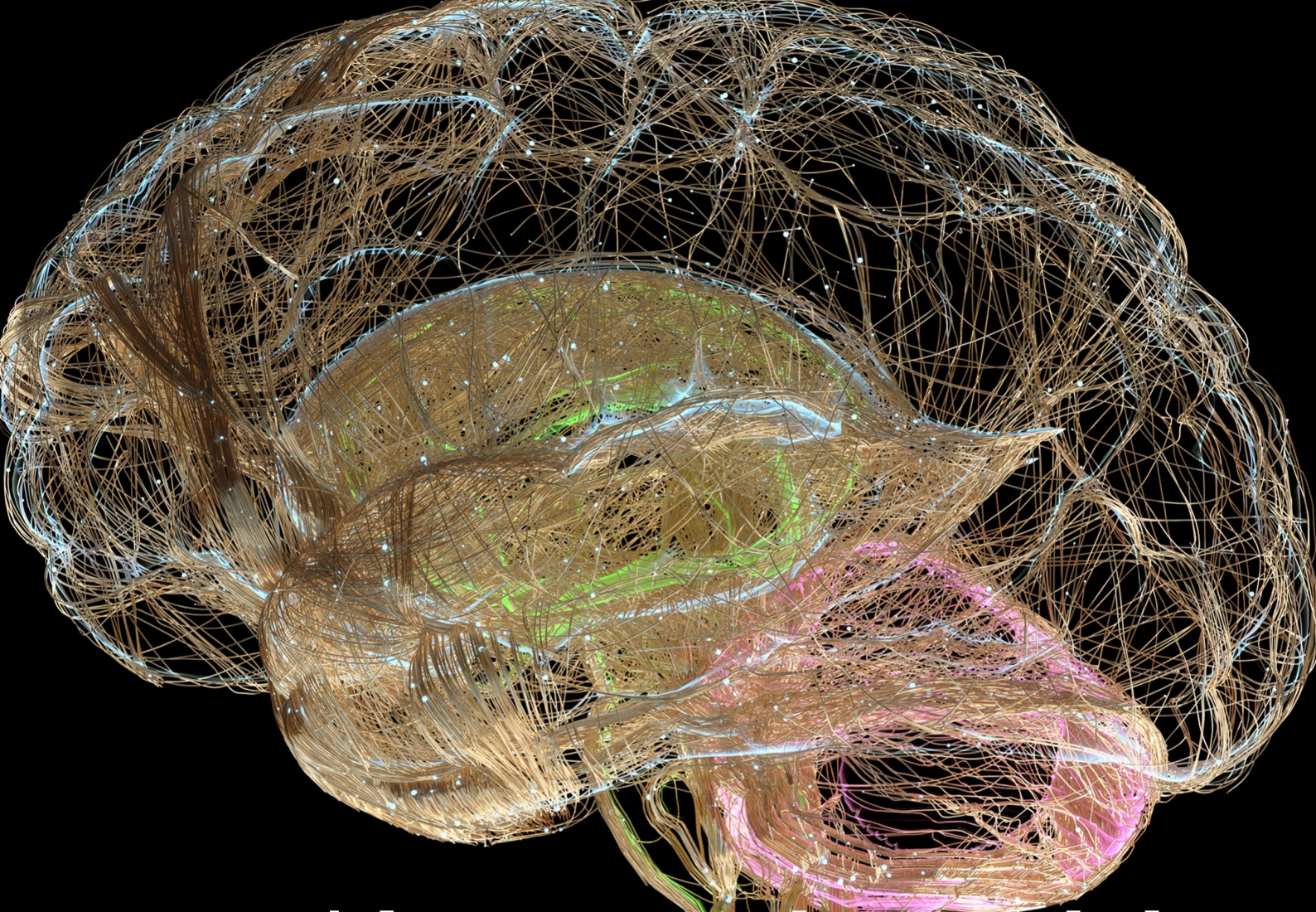

Intracranial pressure pulse morphology and intracranial compliance analysis during liquor drainage in patients with traumatic brain injury

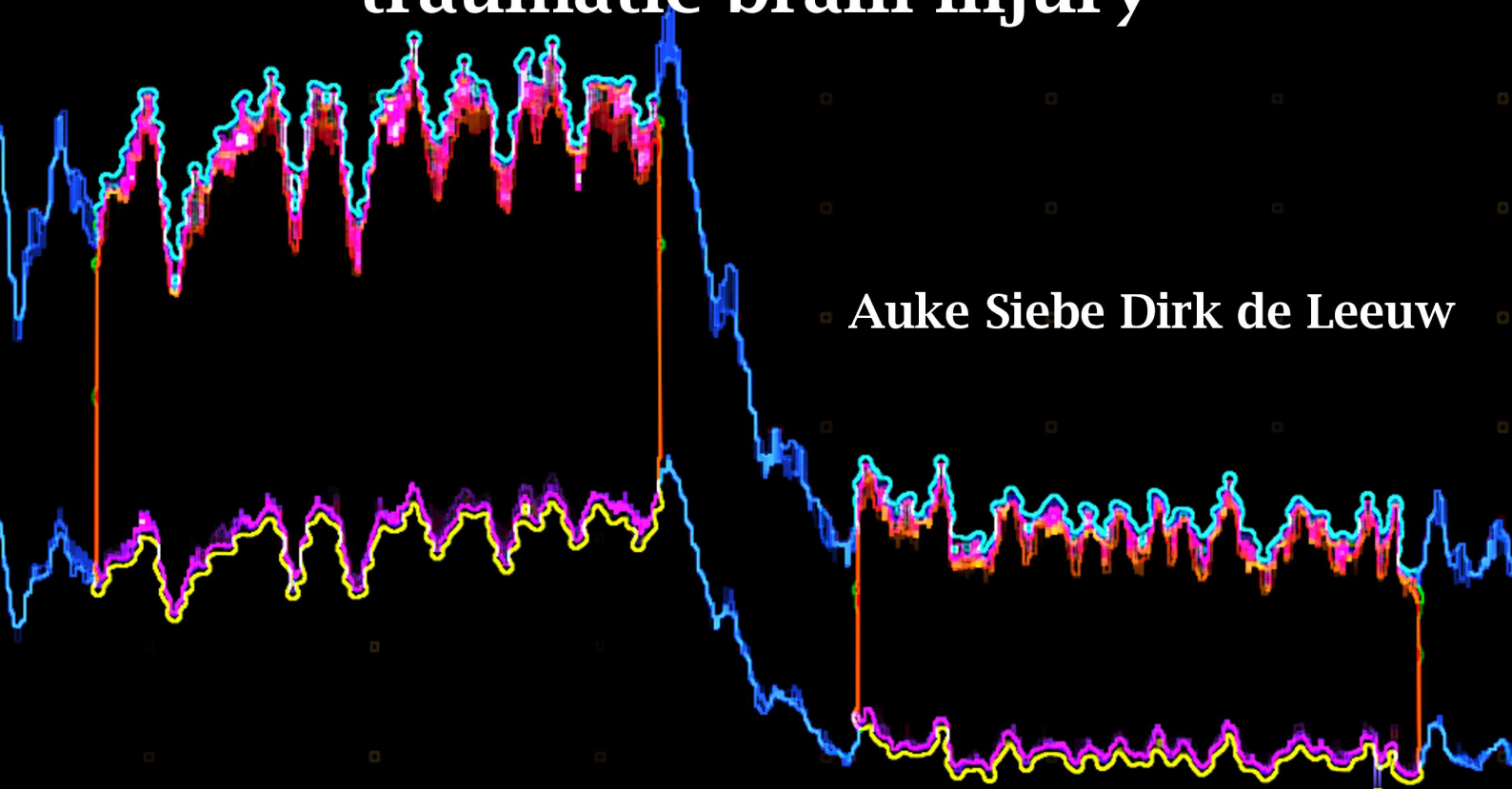

Auke Siebe Dirk de Leeuw

Intracranial pressure pulse morphology and intracranial compliance analysis during liquor drainage in patients with traumatic brain injury

Technical Medicine Graduation Internship
Intensive Care RadboudUMC

A.S.D. de Leeuw

December 2, 2024

Chairman:	Prof.dr.ir. M.J.A.M. van Putten
Medical Supervisor:	Dr. C.W.E. Hoedemaekers
Technical medicine supervisor:	C.R. van Kaam, MSc
Technical Supervisor:	Dr.ir. G. Meinsma
Process Supervisor:	R.J. Lambers, MSc
External member:	Dr. S. Waanders

1 Abstract

Introduction: Traumatic brain injury (TBI) patients often experience increased intracranial pressure (ICP), leading to episodes of intracranial hypertension (IH) and a decreased intracranial compliance (ICC). The correlation coefficient between the amplitude of the ICP pulse and the mean ICP (RAP−index) is the current gold standard for assessing the ICC in TBI patients. A more comprehensive understanding of the ICP pulse morphology, as well as the effectiveness of cerebrospinal fluid (CSF) drainage through an external ventricular drain (EVD), could assist clinical physicians in assessing the ICC of TBI patients. Therefore, this study aims to evaluate various methods of ICP pulse morphology analysis in their ability to assess ICC during consecutive drainage interventions in TBI patients, identifying the most promising clinical useful method in comparison with the gold standard, the RAP−index.
Methods: The ICP pulse morphology was analyzed in the time and frequency domain before and after each drainage event in a cohort of TBI patients undergoing CSF drainage. Additionally, a viscoelastic model was investigated by optimizing parameters in a state−space representation of this model. Data were visualized over time, over a single drainage event as well as in relation with accompanying ICP changes over a single drainage event.
Results: A total of 534 drainage events were analyzed in nine TBI patients. Ten metrics showed significant differences in assessing the ICC and predicting TBI mortality. The second−to−first peak ratio (dP2/dP1 ratio) shows significant differences in TBI mortality at the start of drainage treatment. The third−to−second peak ratio (dP3/dP2 ratio) and the curvature of the first peak (Curv1) both show immediate observable changes after a single drainage event. The viscoelastic model scaled the arterial blood pressure (ABP) pulse to an ICP pulse. Drained volume was precisely measured in one patient, resulting in an exact calculation of ICC for that patient.
Discussion: Due to a cohort of nine TBI patients, the results require validation in a larger patient population. Additionally, since drained volumes were accurately measured in merely one of these patients, verifying this ICC calculation should be prioritized. Next to verifying the results, peak detection in ICP pulses with merged peaks morphologies should be refined as well as the performance of the viscoelastic model.
Conclusion: The second−to−first peak ratio, third−to−second peak ratio and curvature of the first peak of an ICP pulse outperform the RAP−index in assessing the ICC and provide the highest predictive power in TBI mortality. Advancements in ICP pulse morphology and ICC analysis could enable an implementation of bedside monitoring of these metrics, providing crucial insights for clinical physicians in accessing the ICC of TBI patients based on ICP pulse morphology.

2 Table of Contents

List of Figures

List of Tables

3 Introduction

3.1 General background

Annually, 85.000 new cases of patients with traumatic brain injury (TBI) occur in the Netherlands [1]. TBI is defined as an alteration in brain function caused by an external force [2]. This force causes the primary brain injury: the initial insult and the consequences of the immediate parenchymal damage which occurred at the time of the injury. This primary brain injury and those instant consequences cannot be avoided. However, secondary brain injury should be avoided. Therefore, the main focus after the initial is the prevention, identification and management of this secondary brain injury. Secondary brain injury can be caused by cerebral edema, ischemia or the inflammatory response to the primary brain injury. This secondary brain injury could induce intracranial hypertension (IH) [2]. Since IH is a predictor of mortality and poor outcome of TBI patients, intracranial pressure (ICP) is the most common measured cerebral physiological parameter in management of patients with TBI [2]. Hence, a profound understanding of ICP monitoring is needed for the care of all patients with TBI.

The Monro-Kellie doctrine is an essential principle within the TBI pathophysiology. This doctrine states that with an intact skull, the sum of the volumes of brain, blood and cerebrospinal fluid (CSF) is constant at a given ICP[3]. Therefore, an elevation of ICP due to an increase in one of the three volumes, will lead to a compensating response by the other two volumes to lower the ICP [4]. The intracranial compliance (ICC) represents the elasticity of the brain, since compliance is calculated as $C = \frac{\Delta V}{\Delta P}$ where ΔV represents a change in volume and ΔP a change in pressure [5]. This relationship can be seen in figure 1. The ICC permits compensation for volume changes in the ICP up to a certain point, which starts in the yellow zone in figure 1. If the intracranial volume rises beyond this point, this induces a steep rise in ICP. The ICP wave morphology can be seen in each zone in figure 1. Hence, the morphology provides clues to the pressure-volume relationship within the cranium.

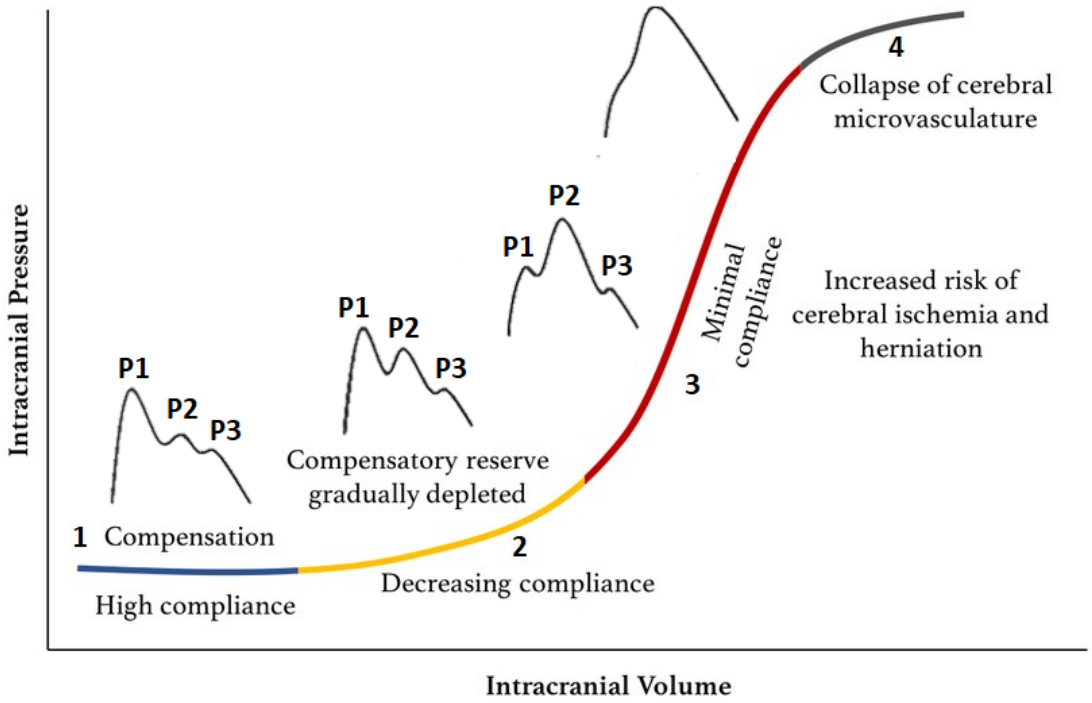

Figure 1: *Pressure-volume curve for the ICP with four indicated zones: (1) a baseline intracranial volume with good compensatory reserve and thus a high compliance (blue zone); (2) gradual depletion of compensatory reserve as intracranial volume increases (yellow zone); (3) poor compensatory reserve and increased risk of cerebral ischemia and herniation (red zone); (4) critically high ICP causing a collapse of cerebral microvasculature and a disturbed cerebrovascular reactivity (grey zone). The ICP morphology can be seen in each zone, with the first (P1), second (P2) and third (P3) peak. ICP: intracranial pressure. Adapted from [6].*

Maintenance of a steady ICP, normally below 15 mmHg in supine adults [2], depends on the three volumes in the intracranial compartment. When elevations of ICP above 22mmHg are present for at least five minutes, this is defined as IH[2]. Pathological IH is present at levels greater than or equal to 20 mmHg, which is commonly treated with a reactive measure such as drainage of CSF or administering osmotic agents [7]. However, numerous cut-off values are proposed for pathological IH within the literature, yet many lack a solid physiological foundation [8, 9]. During sustained elevated levels of ICP, the cerebral perfusion pressure (CPP) can become progressively more compromised which results in higher levels of ICP and could induce signs of herniation in patients [5]. The CPP is the net pressure gradient which drives oxygenated blood towards the cerebral tissue, which is the difference between the mean arterial pressure (MAP) and the ICP: $CPP = MAP - ICP$ [10]. Since a normal ICP is relatively small (below 15mmHg), the CPP is much more dependent on the MAP which has a normal range of 70-100mmHg. Besides the CPP and MAP, the morphology of the ICP waves is of great importance.

3.2 Temporal domain

Waveform morphology

The morphology provides clues to the pressure-volume relationship within the cranium, as can be seen in figure 2. In a normal state of cerebral compliance, the shape of the ICP waveforms consists of three distinct peaks which appear in descending height: P1, P2 and P3 [5]. The first peak is the percussion wave, reflecting arterial pulses of the carotid plexus into the CSF; P2 is the tidal wave, representing arterial pulses which are reflected of brain parenchyma; the last peak is the dicrotic notch, representing the closure of the aortic valve [2].

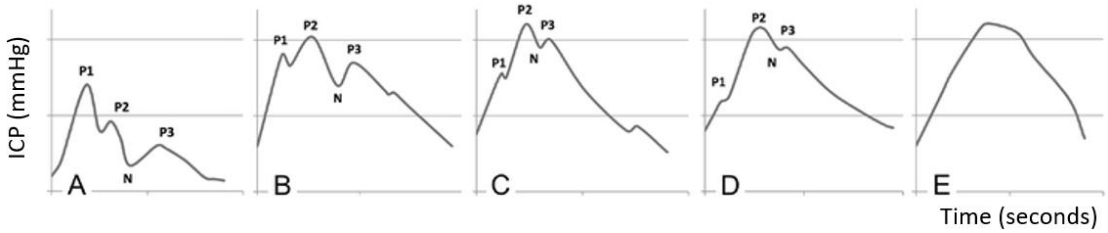

Figure 2: *Change in ICP waveform morphology from normal (panel A) to abnormal (panel E) pressure-volume state within the cranium. Each panel shows a single ICP pulse, where the three characteristic peaks are denoted as P1, P2 and P3. As can be seen in panel A, these three peaks appear in descending height. In abnormal pressure-volume states, when cerebral compliance decreases, P2 becomes progressively more dominant as can be seen in panel B till E. The second peak becomes higher than the first peak showing a more triangular and spikelike shape. The morphology of the ICP signal can thus change in various ways, inducing different shapes and number of peaks of the ICP curve due to merging of two or even all three peaks. ICP: intracranial pressure. Adapted from [11].*

RAP−index

The RAP−index is defined as the correlation between the mean amplitude (Amp_{ICP}) and the mean ICP value (ICP_{mean}) of each individual ICP waveform. The RAP−index can be measured as a moving pearson correlation coefficient over time [12]. The RAP−index is typically calculated over non-overlapping time intervals of 6 to 10 seconds, spanning a total observation period of 300 to 500 seconds [13, 14]. The RAP−index is thus calculated as follows:

$$RAP\text{-}index = \frac{\sum_{i=1}^{n}(ICP_{\text{mean},i} - \overline{ICP_{\text{mean}}})(AMP_{\text{ICP},i} - \overline{AMP_{\text{ICP}}})}{\sqrt{\sum_{i=1}^{n}(ICP_{\text{mean},i} - \overline{ICP_{\text{mean}}})^2 \sum_{i=1}^{n}(AMP_{\text{ICP},i} - \overline{AMP_{\text{ICP}}})^2}} \quad (1)$$

where:

$ICP_{\text{mean},i}$ is the mean intracranial pressure at index i

$\overline{ICP_{\text{mean}}}$ is the average mean intracranial pressure over a certain time window

$AMP_{\text{ICP},i}$ is the mean amplitude of the ICP wave at index i

$\overline{AMP_{\text{ICP}}}$ is the average mean amplitude of the ICP wave over a certain time window

n is the number of time points within the moving window.

An RAP−index value close to 0 indicates an ideal compensatory reserve of the brain, since changes in the AmpICP are not induced by oscillations in mean ICP (so there is little to no correlation between the AmpICP and the mean ICP). This indicates that the cerebral autoregulation is intact, since there is a coordinated relationship between ICP and the AmpICP. Within the graph of the pressure-volume relationship, this correlates with the area before the steep rise as can be seen as region 1 in figure 3. An RAP−index value larger than zero, often close to 1 in a patient following head injury and subsequent brain swelling [15], indicates a decreased compensatory reserve of the brain. This is due to the fact that changes in the mean ICP induce corresponding changes in the AmpICP (zone 2 and 3 in figure 3). Within this range, the cerebral autoregulatory mechanisms remain active. However, negative values of the RAP−index indicate a disturbed cerebrovascular reactivity, which correlates with the right zone in the sigmoid graph in figure 3. This indicates that when the RAP−index falls below 0, the cerebral autoregulation is disrupted. The right panel of figure 3 shows the relation between the amplitude of the ICP pulse and the mean ICP more clearly. It has been shown that the RAP−index is an accurate measure of the ICC [16], therefore the RAP−index is used as an indicator to access in which zone the patient on the pressure-volume curve currently is. It should be noted that the RAP−index is susceptible to baseline effect errors, e.g. spontaneous mean ICP shifts or the effect of the ICP sensor location [17, 18]. There is no consensus in the literature whether the RAP−index is more accurate in assessing cerebral compensatory reserve compared to the AmpICP [6]. However, recent studies showed that the RAP−weighted mean ICP outperform standard mean ICP regarding the prediction of the outcome of a patient after TBI and thus highlighting the importance of the RAP−index [19, 13, 14]. The RAP−weighted mean ICP is calculated as follows:

$$RAP_{\text{weighted mean ICP}} = ICP_{\text{mean},i}(1 - RAP\text{-}index) \tag{2}$$

where:

$ICP_{\text{mean},i}$ is the mean intracranial pressure at index i

RAP_{index} is the RAP index caculated for this window.

Both the RAP−index and AmpICP are currently used as markers for intracranial physiological parameters, however, neither have yet been used as a marker to guide clinical management [18].

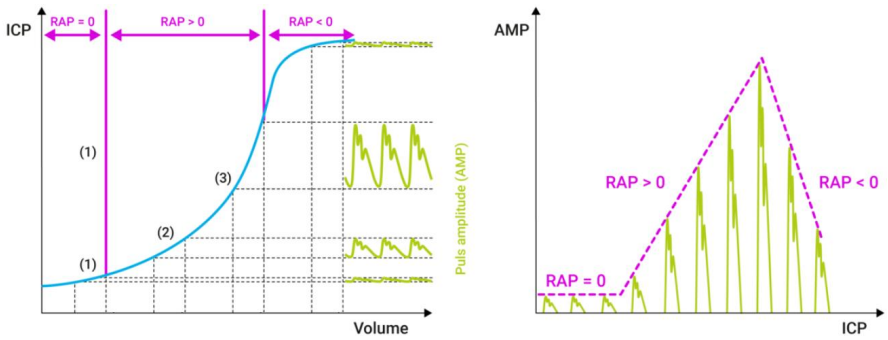

Figure 3: *Relation between the value of the RAP−index and the pressure-volume curve of the ICP in the left panel of this figure. On the x−axis the increasing cerebral blood volume is shown. Identical increases in volume on the x−axis are related with different pulse amplitudes of the ICP pulse, as can be seen on the right side of this panel. In the right panel, the relation between the amplitude of the ICP pulse and the mean ICP can be observed clearly. ICP: intracranial pressure. Figure adapted from Czosnyka and Pickard (2004), with adjustments for clarity [15].*

MOCAIP metrics

In order to analyze the individual waveform of the ICP in more detail, Hu et al. created an algorithm to quantify the waveform morphology by means of 24 metrics for a complete characterisation of morphology termed Morphological Clustering and Analysis of Intracranial Pressure (MOCAIP) [7]. These 24 metrics give insight in the amplitude, latency, curvature, slope and decay as can be seen in figure 4.

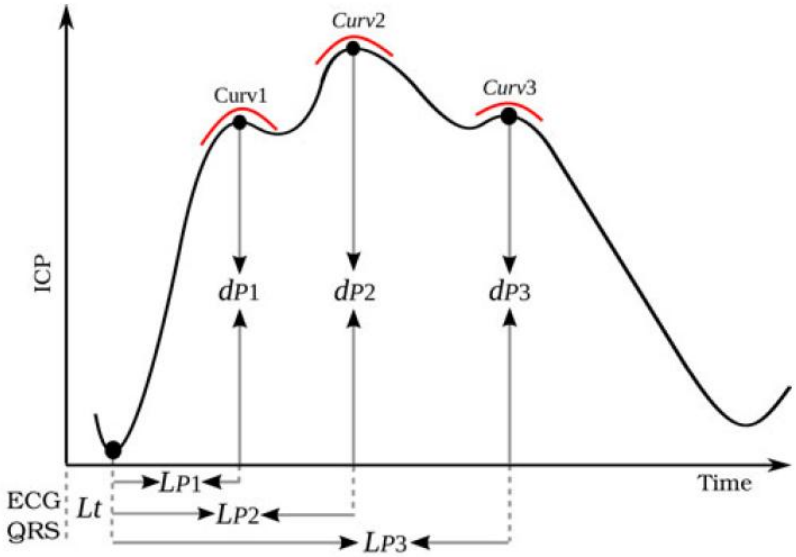

Group		MOCAIP Metrics
Amplitude	Value	$dP_1, dP_2, dP_3, diasICP, mICP$
	Ratio	$dP_2/dP_1, dP_3/dP_1, dP_3/dP_2$
Latency	Value	L_T, L_1, L_2, L_3
	Ratio	$L_2 - L_1, L_3 - L_1, L_3 - L_2$
Curvature	Value	$\mathrm{Curv}_1, \mathrm{Curv}_2, \mathrm{Curv}_3, \mathrm{Curv}_m$
	Ratio	$\mathrm{Curv}_2/\mathrm{Curv}_1, \mathrm{Curv}_3/\mathrm{Curv}_1, \mathrm{Curv}_3/\mathrm{Curv}_2$
Slope		$(P_1 - diasICP)/L_1$
Decay		L_x where $dP_x = 0.37dP_3$

Figure 4: *The 24 morphological metrics which can be extracted from the ICP signal using the configuration of the three peaks using the MOCAIP algorithm. ICP: intracranial pressure, MOCAIP: Morphological Clustering and Analysis of Intracranial Pressure [20].*

Each metric of this algorithm has been researched regarding their importance in forecasting ICP elevation with the exception of the onset latency (L_T: the latency between the peak of the ECG QRS peak and the start of the ICP pulse, see figure 4), the mean and the diastolic ICP. Of the other 21 MOCAIP metrics, the ten most predictive MOCAIP metrics for different pre-IH segments are shown in table 1.
However, an analysis regarding the changes in ICP waveform morphology and what these changes correspond to remains unexplored [7].

Table 1: *List of the top 10 most predictive MOCAIP metrics for differentiating pre-IH segments from normal segments. The onset latency (L_T), mean and diastolic ICP were excluded in this analysis. Each row represents the values of the MOCAIP metrics corresponding to 0, 5, 20 and 35 minutes prior to IH. IH: intracranial hypertension, ICP: intracranial pressure, MOCAIP: Morphological Clustering and Analysis of Intracranial Pressure [21].*

Pre IH	**Top 10 most predictive MOCAIP metrics**									
0	$Curv3$	$\frac{dP2}{dP1}$	$\frac{dP3}{dP1}$	$dP1$	$\frac{Curv2}{Curv1}$	$dP3$	$Slope$	$\frac{dP3}{dP2}$	$CurvM$	Lx
5	$Curv2$	$Curv3$	Lx	$dP3$	$\frac{dP2}{dP1}$	$CurvM$	$dP2$	$\frac{dP3}{dP2}$	$\frac{dP3}{dP1}$	$dP1$
20	$Curv2$	$\frac{dP3}{dP2}$	Curv3	$\frac{dP3}{dP1}$	Lx	$\frac{dP2}{dP1}$	$\frac{Curv2}{Curv1}$	$dP1$	$Slope$	$dP2$
35	$Curv3$	$Curv2$	$CurvM$	$\frac{Curv3}{Curv1}$	$\frac{Curv3}{Curv2}$	$\frac{dP3}{dP2}$	$\frac{dP3}{dP1}$	$dP1$	Lx	$\frac{dP2}{dP1}$

A pilot study researched these metrics in four TBI patients with a total of 321 drainage moments [22]. Each metric was calculated during a 30 second interval before and after drainage. This resulted in MOCAIP metrics before and after drainage as well as their difference over drainage. Each peak as well as the height ratio of these peaks, especially dP2/dP1 and dP3/dP1, showed a large difference over drainage. The slope of the first peak also showed a large difference over drainage. Next to these differences, the trend of the peak height differences over consecutive drainage moments appeared to be different between the 2 patients with a good outcome compared to the 2 patients with a poor outcome. The mean ICP after an ineffective drainage intervention showed a more rapid increase than after an effective drainage intervention (a drainage moment is classified effective if drainage resulted in stable ICP's without a new interventions for at least 40 minutes). The dP2/dP1 peak ratio exhibited a similar faster increase after an ineffective drainage compared to an effective drainage intervention which showed a more stable dP2/dP1 ratio after drainage. Therefore, these MOCAIP metrics might have a predictive value regarding the outcome of a TBI patient as well as providing the clinical physician with crucial insights for IH in the Intensive Care Unit (ICU).

3.3 Frequency domain

Instead of analyzing the ICP waveform in the time domain, such as the MOCAIP algorithm, one could also analyze the ICP waveform in the frequency domain. Using the Fast Fourier transform (FFT), the ICP signal can be decomposed into several sinusoidal components (figure 5b)[23]. This can be represented within a single-sided FFT amplitude spectrum, in order to visualize the amplitude of each frequency (figure 5c)[23]. The amplitude of the ICP waveform (AmpICP) can then easily be extracted, since this is the amplitude of the most prevalent frequency (the fundamental harmonic) (figure 5d)[23]. The correlation between this AmpICP and the mean ICP value is the earlier discussed RAP-index [12].

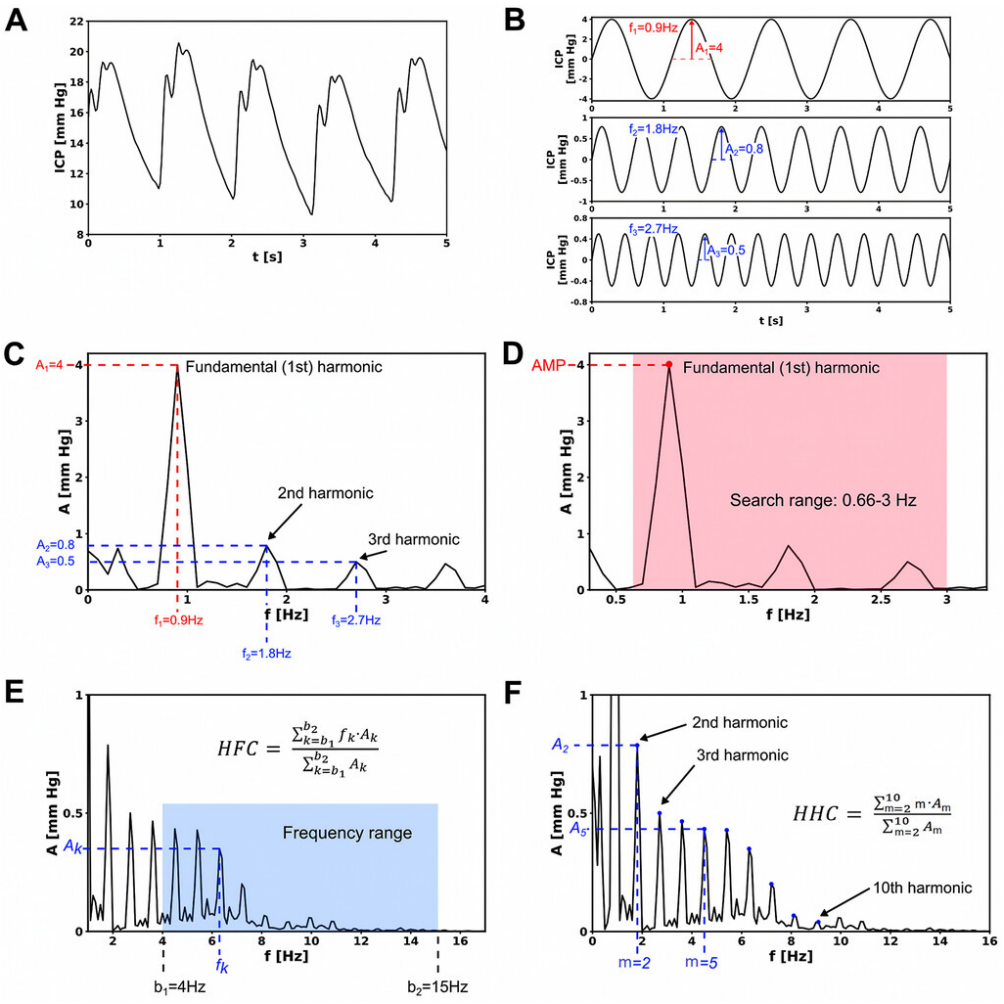

Figure 5: *Different methods for analyzing the ICP waveform within the frequency domain. Panel **A**: ICP signal with several ICP waveforms over a 5 second window. Panel **B**: The same ICP signal as in panel A, but deconstructed in several sinusoidal waves with different amplitudes (A) in mmHg and frequencies (f) in Hz. The fundamental component is illustrated in red (i.e., the "strongest" component of the pulsatile ICP signal corresponding to heart rate as well as specific spectral components, called harmonics, which are multiples of the fundamental frequency are given in blue (the 2nd and 3rd harmonics are shown). Panel **C**: The FFT represents the ICP signal's amplitude as a function of frequency, shown as the single-sided FFT amplitude spectrum. Each of the 3 sinusoidal components from panel B is visible as a local maximum (peak). Panel **D**: The AMP is calculated as the amplitude of the fundamental (1st) component by finding the maximum of the amplitude spectrum in the range corresponding to heart rate in an adult human (40–180 bpm, or 0.67–3 Hz). The maximum is marked by a red dot. Panel **E**: HFC is calculated from the spectral content contained within the frequency range from 4 Hz to 15 Hz (marked by the blue rectangle). Each sample within this range is characterized by frequency f_k with the corresponding amplitude A_k (see equation 3 and 4). HFC is the amplitude-weighted average frequency described by the equation shown in the panel. It can be linked to the center of mass of the spectrum, where mass corresponds to the amplitude of each frequency component. **F**: In contrast to HFC, HHC is not calculated from all the samples within a given frequency range, but only from the harmonics numbered from $m = 2$ to $m = 10$ (i.e., from 2 to 10 times the fundamental frequency). It is expressed in harmonic number rather than in Hertz and is theoretically less dependent on heart rate than HFC. ICP: intracranial pressure, t: time, Hz: Hertz, FFT: Fast Fourier Transform, AMP: amplitude of the ICP waveform, bpm: beats per minute, HFC: high frequency centroid, HHC: higher harmonics centroid. [23].*

The aforementioned frequency and corresponding amplitude at a certain index are calculated as follows:

$$f_k = \frac{k \cdot F_s}{N}, \quad \text{for} \quad k = 0, 1, 2, \ldots, \frac{N}{2} \tag{3}$$

$$A_k = \frac{2}{N} |X_k|, \quad \text{for} \quad k = 1, 2, \ldots, \frac{N}{2} \tag{4}$$

where:

F_s is the sampling frequency

N is the total number of samples

X_k is the FFT result at index k.

High Frequency Centroid

The first frequency domain metric is the high frequency centroid (HFC) [24]. The HFC value is the amplitude-weighted average frequency, calculated within the frequency range of 4 to 15 Hz as can be seen in figure 5e. Each sample within this frequency range is characterized by a frequency f_k (in Hz, see equation 3) corresponding to a certain index k and amplitude A_k (see equation 4). Therefore, the HFC is a metric in Hertz and is calculated as follows:

$$HFC = \frac{\sum_{k=b_1}^{b_2} f_k \cdot A_k}{\sum_{k=b_1}^{b_2} A_k} \tag{5}$$

where:

k is the index

f_k is the frequency for a certain index k

A_k is the spectral amplitude of the corresponding frequency at index k

$b_1 \& b_2$ are the indexes of a certain bin, in this case between 4 Hz and 15 Hz.

Bray et al. already showed in 1986 that a HFC value of the ICP wave around 7 Hz is considered normal, whereas an increase up to 9 Hz correlates with an exhausted compensatory reserve [25]. Several years later, Robertsen et al. demonstrated that increased HFC correlates with higher mortality as well as occurrence of IH [24]. Moreover, opposite direction of changes in HFC could differentiate between transient and refractory hypertension episodes [26]. HFC can therefore be a measure of intracranial compliance [24].

Higher Harmonics Centroid

A slightly different centroid metric, the higher harmonics centroid (HHC), is less dependent on the heart rate than the HFC [27]. The HHC is not calculated from all frequencies within a certain frequency range (as is the case with the HFC, which includes the fundamental cardiac frequency), but is calculated only from several harmonics as can be seen in figure 5f. Therefore, the HHC is a metric which represents an index and is calculated as follows:

$$HHC = \frac{\sum_{m=b_1}^{b_2} m \cdot A_m}{\sum_{m=b_1}^{b_2} A_m} \tag{6}$$

where:

m is the harmonic number, representing a multiple of the fundamental frequency

A_m is the spectral amplitude at harmonic number m

$b_1 \& b_2$ are the bin indexes, in this case a bin between the 2nd and 10th harmonic number m.

Using the range in harmonic numbers for analysis, which are multiples of the fundamental frequency, rather than using frequencies in Hz as with the HFC, HHC takes variations in heart rate not into account. Therefore, an increase in HHC could be interpreted as an increase in the distortion of the ICP waveform (irrespective of the heart rate) [12]. When the HHC is calculated from the 2nd through the 10th harmonic of an ICP waveform, the HHC was shown to be positively correlated with the mean ICP in TBI patients [28]. A recent study showed that, when HHC was compared to HFC in the same dataset, elevated HFC indeed correlates with mortality and a poor outcome whereas HHC may serve as a reliable early indicator of IH [23]. This early predictor possibility is based on the occurrence of a 'breakpoint' in the relation between HHC and the mean ICP, visible at a level of around 25-30 mmHg as can be seen in figure 6. Changes in the ICP pulse wave morphology can also be observed in this figure. Thus, due to accompanying change in HHC compared to a change in the ICP waveform morphology, HHC correlates with the intracranial compliance. However, the designated breakpoint and the green lines in Figure 6 lack clear distinction. It could be argued that alternative lines, and consequently, different breakpoints, could similarly be represented in this figure.

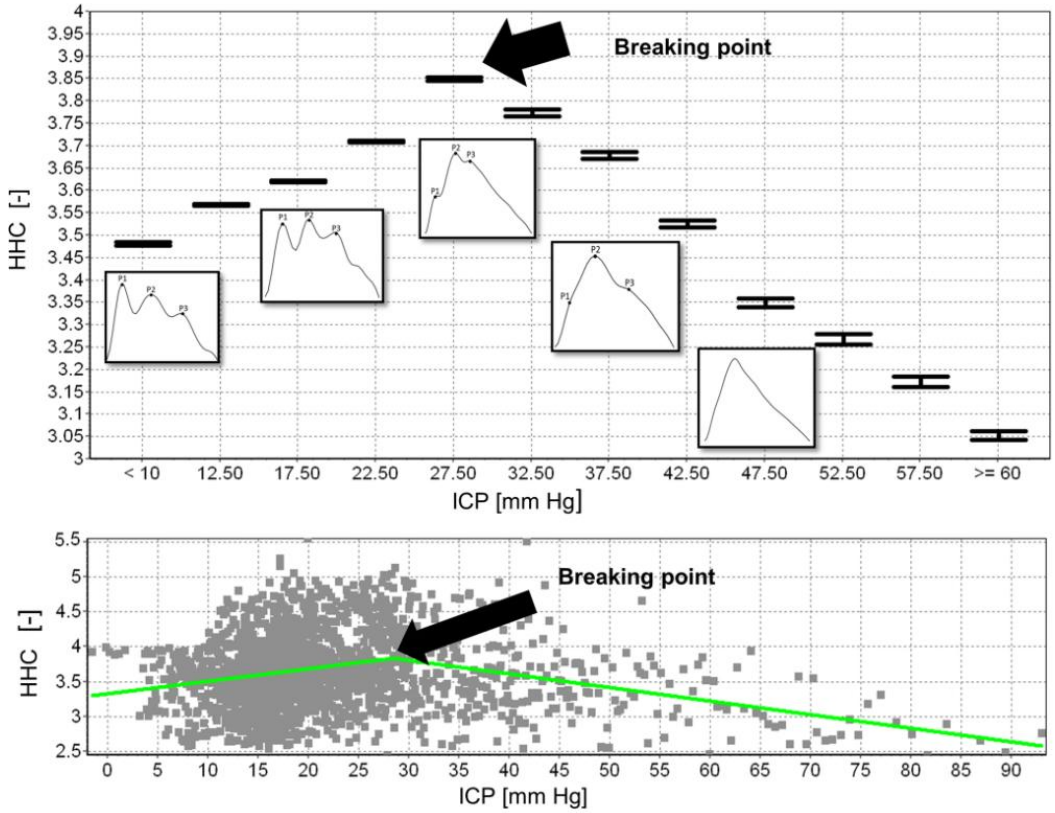

Figure 6: *The HHC error bar chart (upper panel) and the ICP-HHC scatter diagram (bottom panel) plotted for pooled data (26 ICP recordings). HHC increases with rising ICP up to approximately 27.5 mm Hg (a breaking point) and then decreases with a further ICP elevation. The change in the shape of the ICP pulse waveform (from the typical three-peak appearance to triangular shape) initially causes the HHC to increase and then, after crossing the breakpoint, the HHC eventually decreases due to the lower content of higher frequencies. ICP: intracranial pressure; HHC: higher harmonics centroid. Symbol [–] denotes a dimensionless unit. [28].*

There lie challenges within the frequency domain analysis, due to the variability of the ICP pulse shape over time as well as the nonlinear dependence on mean ICP and cerebrospinal compliance [23]. The use of the Fourier transform needs some requirements, such as a sampling frequency of at least twice the highest frequency in the signal and a periodic and stationary signal which indicates that the spectral content remains relatively unchanged over a certain time period. During continuous ICP monitoring in the ICU, with frequent alterations in heart rate and rapid changes in the patient's condition, the ICP signal might not always be stationary and thus imposing several challenges for analysis. Next to these challenges, the values of HFC and HHC do not directly describe the shape of the waveform in the time domain, thereby making such values difficult to interpret for the clinical physician [12].

3.4 Viscoelastic model

Another method for analyzing the compliance of the brain within TBI patients, is to model the brain physiology. Doron et al [29] developed a model which includes cerebral interstitial fluid (ISF) flow within brain tissue as well as the interactions of ISF flow with cerebrospinal fluid (CSF) flow and the cerebral blood flow (CBF). This model is based on an electrical analog circuit with four intracranial compartments: the subarachnoid space, brain, ventricles as well as the cerebral vasculature and the extracranial spinal thecal sac. Nassir et al [30] refined this model by adding viscoelastic elements, since models such as the model of Doron et al [29] did not incorporate anatomical elements which could affect the transformation of the arterial bloodpressure (ABP) waveform into the ICP waveform. This model can be found in figure 7.
Nassir et al. hypothesized that the transformation from the ABP waveform to the ICP waveform could be explained by adding those viscoelastic elements. Thus, by combining elastic and viscous elements, certain intracranial tissues as well as the cerebrovascular tree could be modelled more accurately. These viscoelastic elements affect the propagation velocity of the ABP through brain-tissue as well as the velocity of reflected pressure waves that interfere with those propagating waves, thereby resulting in delays in the propagation as well as in reflecting pressure waves. Therefore, this could be the cause of the ICP waveform morphology with its distinctive three peaks. The results of Nassir et al. [30] showed that the addition of viscoelastic elements indeed caused a more accurate ICP waveform morphology compared to the model od Doron et al. [29] without those elements. By using this viscoelastic model, difficult-to-measure but clinically vital information such as the brain compliance could be estimated in TBI patients. Therefore, using this model in TBI patients could significantly benefit clinical physicians.

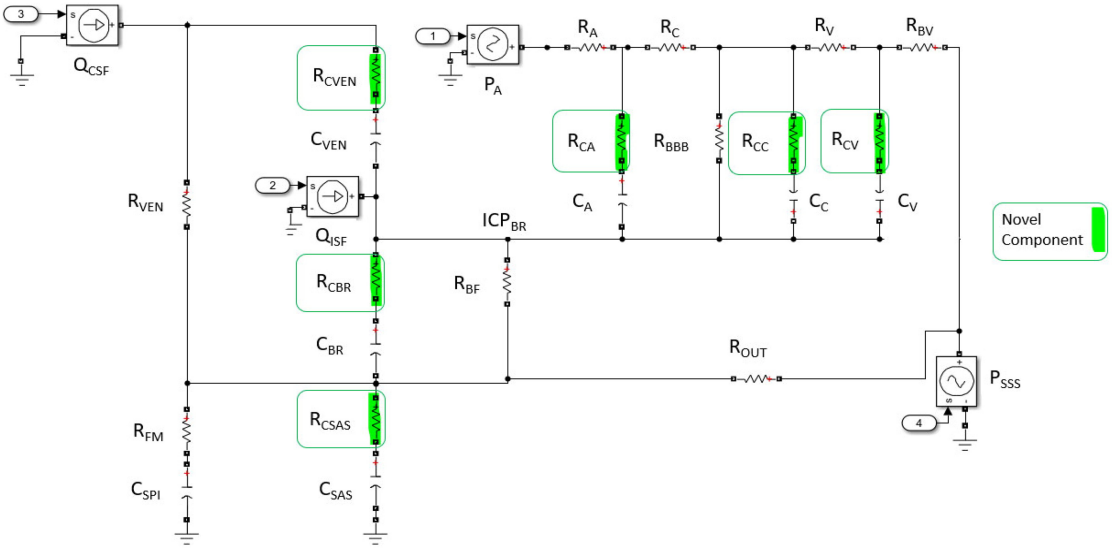

Figure 7: *The electrical analog circuit for the brain physiology with viscoelastic components (represented in green). The model compartments are: arterial–arteriolar compliance (CA); brain compliance (CBR); capillary compliance (Cc); subarachnoid space compliance (CSAS); spinal thecal sac compliance (CSPI); venous compliance (CV); ventricular compliance(CVEN); brain ICP (ICPBR); arterial pressure (PA); superior sagittal sinus pressure (PSSS); CSF production rate (QCSF); cerebral interstitial fluid production rate (QISF); arterial–arteriolar resistance to flow (RA); resistance across the brain–blood barrier (RBBB); resistance to bulk flow of cerebral interstitial flow through the brain (RBF); bridging veins resistance to flow (RBV); capillary resistance to flow (RC); viscous forces of arteries and arterioles compartment (RCA); viscous forces of brain tissue compartment (RCBR); viscous forces of capillaries compartment (RCC); viscous forces of subarachnoid compartment (RCSAS); viscous forces of veins compartment (RCV); viscous forces of ventricles compartment (RCVEN); resistance to CSF flow through the foramen magnum (RFM); resistance to CSF reabsorption and to bulk flow in the subarachnoid space (ROUT); venous resistance to flow (RV); resistance to CSF flow in the ventricles (RVEN) [30].*

3.5 Clinical relevance

To summarize, several methods are available for assessing the ICP waveform morphology and thus assessing the intracranial compliance. Without the need of analyzing each individual waveform, the viscoelastic model might be an option for assessing the ICP timeseries as a whole and thereby providing insights in the ICC. The clinical significance of assessing the compliance of the brain in TBI patients of each of those methods in relation with each other within the same dataset has not yet been studied in existing literature. Furthermore, there still is an unmet need for a clinically acceptable method for acquiring intracranial compliance[31]. Hence, investigating these methods in terms of their efficacy in assessing ICC holds profound clinical significance.

A better understanding of ICC of the patient is needed, since this can be a more reliable target than ICP alone [32]. For instance, when a patient's working point in the pressure-volume curve (figure 1) is within zone 2, the ICC is already decreasing without a significant rise in ICP level (therefore, as explained in the general background, a cut-off value for the ICP is an oversimplification for all TBI patients). Due to this discrepancy between ICP and ICC, other methods

besides an analysis on the morphology of the ICP waveform are researched to monitor the oxygenation and compliance of the brain. Oximetry probes for instance, could provide information regarding local brain tissue oxygenation ($PbtO_2$) [33]. The use of ultrasound, such as duplex and trans cranial doppler (TCD), could provide information regarding the cerebral autoregulation (currently researched by other M3 Technical medical students in the RadboudUMC) [33]. Even the automated neurological pupil index (NPi) is a reliable metric in observing a worsening neurological condition as a consequence of IH [33]. Due to these various monitoring methods, each accessing a different relevant aspect in TBI patients, a diagnostic model is proposed by *Godoy et al.* to integrate the monitoring of the ICC [33]. The methods in this model all have a solid rationale for their use, however, large trials for these methods remain lacking [34, 35]. However, this proposed model incorporating several monitoring methods highlights the need for an accurate method for acquiring ICC in TBI patients. Due to the fact that ICP measurement is the most common measurement on the ICU in TBI patients, this research will focus on the monitoring methods based on the ICP.

3.6 Aim of this study

Through waveform morphology analysis in the temporal domain as well as in the frequency domain, combined with a viscoelastic model to analyze the ICP waveform, this research aims to give an overview of the clinical significance of each method in analyzing the ICC in TBI patients on the ICU. This will be achieved by comparing these methods with each other in terms of their response/change patterns over consecutive drainage interventions. Therefore, this study holds significant clinical importance as it aims to provide crucial insights for clinical physicians regarding several methods to assess the compliance in TBI patients.
Given that the RAP-index provides insights into a patient's 'working point' on the pressure-volume curve (see figure 1) and is commonly utilized in clinical practice, whereas the other methods have limited clinical use and a less direct association with the pressure-volume curve, the RAP-index will serve as the 'golden standard' metric in this research. The proposed aim of this research is thus to address the following research-question:

"In TBI patients admitted to the ICU, how do various methods of ICP waveform morphology analysis differ in their ability to assess brain compliance over consecutive drainage interventions compared with the RAP-index, and which method shows the most promising clinical utility for this purpose?"

For a better and more robust 'golden standard', the following method was proposed at the start of this study. When TBI patients arrived on the ICU, exactly 10cc (or another standard amount of volume) was drained through the EVD. This enables an exact calculation of the brain compliance within each drainage moment, which could have been a better 'golden standard' than the RAP-index. However, only one patient arrived on the ICU during the final weeks of this study. This patient is included in the analysis of this study, however, the RAP-index is used as golden standard within this study in all patients.

4 Methods

4.1 Population and Data collection

The data in this study consisted of 9 TBI patients admitted to the ICU of the RadboudUMC Hospital (Nijmegen, The Netherlands). All patients had an intraparenchymal probe and an external ventricular drain (EVD). Of these patients, four survived the TBI whereas 5 did not survive. The data consisted of continuous ICP measurements with a sample frequency of 125Hz and accompanying notes of the nurses with drainage timestamps and estimated amounts of drained CSF. Data was available as high resolution data in an Hierarchical Data Format version 5 (hdf5), which is analyzed in Python using Spyder version 5.5.1. [36].

4.2 ICP pulse segmentation

The running mean of the ICP signal was calculated using a second order low pass butterworth filter, with a cut of frequency of 0.1Hz. Using this mean ICP, the largest decrease of ICP within a 30 second window in the selected time range was calculated (indicating the drainage moment). Then a region of 300 seconds before and after the drainage moment was automatically selected (Figure 8). The region before drainage was automatically selected when a drop of 3mmHg was detected within 30 seconds, marking the end point of the 300 second region before drainage. In a similar way, the region after drainage was selected when the mean ICP did not change more than 2mmHg over 30 seconds (thereby marking the start of the region after drainage). These values, 3mmHg for the region before and 2mmHg for the region after drainage, were choses arbitrary in order to analyse all drainage events consistently.
Within each region of 300 seconds before and after drainage, the peaks of the waveform were found using the maximal curvature k, calculated as the following metric as mentioned by Hu et al[37]:

$$|k(n)| = \frac{|x(n)''|}{(1 + (x(n)')^2)^{3/2}} \tag{7}$$

where:

$k(n)$ is the curvature at time step n

$x(n)''$ is the second derivative of the ICP at time step n

$x(n)'$ is the first derivative of the ICP at time step n.

The obtained peak indices based on the curvature were deleted if the value ($k(n)$) was below the arbitrary chosen threshold of 85% of the mean ICP value in that wave segment. This is done, since the peak indices of P1, P2 and P3 are expected to be above the mean. However, a visual inspection of each region before and after drainage was done in order to check whether this threshold should be lowered for a specific drainage moment when there were peaks present below the threshold. If present, these alterations were noted at the drainage timestamps. After this peak detection, the region of 300 seconds is segmented in separate waves. This is done using the `find_peaks` function from the Python library[36], to select the lowest peaks as starting points for each wave segment. If there were more than three peaks detected in a single wave segment, those with the lowest curvature value were deleted.

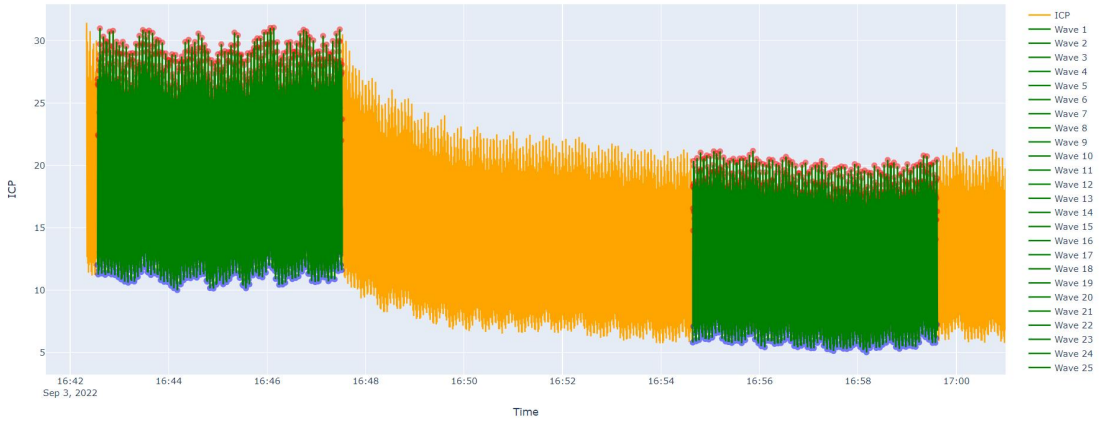

(a) *Both selected regions of 300 seconds before and after drainage can be seen. The orange signal indicates the ICP, each segmented wave is indicated in green and the accompanying peaks in red. The start index of each wave is indicated in blue.*

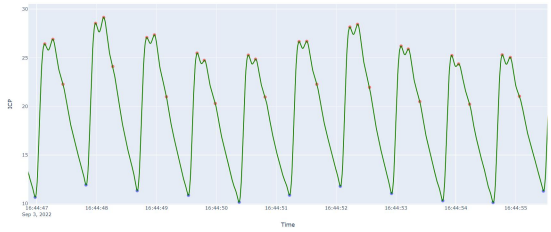

(b) *Zoomed-in region of ten ICP pulse waves before drainage, where the three peaks can be seen as red dots and the start of each wave indicated by a blue dot.*

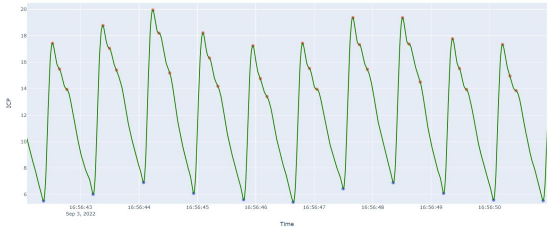

(c) *Zoomed-in region of ten ICP pulse waves after drainage, where the three peaks can be seen as red dots and the start of each wave indicated by a blue dot.*

Figure 8: *Example of an overview and zoomed-in images of the ICP during a drainage moment in a TBI patient. ICP: Intracranial pressure. TBI: Traumatic brain injury.*

4.3 Temporal metrics

Then for each wave-segment the MOCAIP metrics were calculated. For each MOCAIP metric a median value was calculated before and after drainage, which was then saved together with the number of waves used for calculating this median value for each metric. The data was saved in three groups based on the number of peaks present in each wave-segment. This resulted in a dataframe with values for each MOCAIP metric before and after drainage. In order to identify changes of the MOCAIP metrics of all patients over a drainage moment, the difference of each

metric is given by:

$$\Delta\text{median MOCAIP value} =$$

$$\text{median MOCAIP value}_{\text{after drainage}} - \text{median MOCAIP value}_{\text{before drainage}} \quad (8)$$

Next to the MOCAIP metrics, the RAP-index was calculated for each 300s period before and after drainage. Within the 300s period, all ICP waves were divided into 30 groups of around 10 seconds. Each group contained complete ICP wave-segments, resulting in 30 groups with around 10 ICP wave-segments. For each of those 30 groups within the 300s period, the mean ICP value was calculated as well as the mean amplitude of the ICP wave. Therefore, this resulted in 30 values for the mean ICP as well as 30 values for the amplitude of the ICP wave before and after drainage. The RAP-index was then calculated as the Pearson correlation of those 30 values before as well as after drainage, resulting in one RAP-index value before drainage as well as one RAP-index value after drainage (see equation 1). Then, the RAP-weighted mean ICP value (see equation 2) is also calculated before and after drainage.

For the drainage moment itself, several metrics were also calculated:

- The normalized decrease rate during drainage. After calculating the linear decrease rate (dividing the median ICP difference over drainage by the drainage time), this decrease rate is normalized by dividing the decreate rate with the median ICP before drainage. This normalisation is done in order to compare this decrease rate between patients.
- The normalized area under the curve (AUC) of the drainage moment. After all ICP values during the drainage are divided by the initial ICP value at the start of the drainage, these ICP values are normalized. Then the AUC is calculated using the trapezoidal rule over this normalized pressure segment.
- The half-life of the drainage moment. In order to determine the half-life of the drainage moment, an exponential decay curve is fitted on this drainage moment:

$$ICP(t) = ICP_0\, e^{-\lambda t} \quad (9)$$

where:

$ICP(t)$ is the intracranial pressure at time t

ICP_0 is the intracranial pressure at start of the drainage event

λ is exponential decay constant

t is the time.

The value of the exponential decay constant (lambda) is then used to calculate the half-life of the drainage event:

$$t_{1/2} = \frac{\ln(2)}{\lambda} \quad (10)$$

where:

$t_{1/2}$ is the half-life of the drainage event

λ is exponential decay constant.

4.4 Frequency metrics

Using the same 30 groups of 10 complete ICP wave-segments before and after drainage as used for calculating the RAP-index, the HFC, HHC as well as the fundamental frequency and fundamental amplitude were determined. For each group of 10 complete ICP wave-segments, the Fast Fourier Transform (FFT) is applied. Using a frequency range between 4 and 15 Hz, as is explained in figure 5E, the HFC was calculated for each group thereby resulting in 30 values for the HFC before and after drainage.
Then, the frequency peaks of the FFT were numbered. The first peak corresponds to the fundamental frequency (x-value) as well as the fundamental amplitude (y-value). Both these values were saved of each group. Using the second till 10th numbered peak of the FFT, the HHC was calculated for each group (as explained in figure 5F).
In order to research the common 'power' value as used in e.g. a power spectral density, the amplitude within the numerator of both the HFC and HHC were squared. Thus, for both the HFC and HHC a new metric (HFC−power and HHC−power) was calculated as well for each group before and after drainage.

4.5 Viscoelastic model

It was not straightforward to implement the physiological model of Nassir et al. [30] within Python, due to the fact that the differential equations were missing in this paper. Furthermore, in the paper of Doron et al [29] no differential equations were found. After trying to reach the authors of both papers, which did not result in a response, the choice was made to derive those differential equations from the electrical circuit. The following relations were used to derive these differential equations:

Kirchhoff's Current Law (KCL) states that the sum of currents entering a node is equal to the sum of currents leaving the node:

$$\sum I_{\text{in}} = \sum I_{\text{out}}. \tag{11}$$

where:

I_{in} are the currents entering a node

I_{out} are the currents leaving a node.

Kirchhoff's Voltage Law (KVL) states that the sum of the electrical potential differences (voltage) around any closed loop within the circuit is zero:

$$\sum V = 0. \tag{12}$$

where:

V is the electrical potential difference.

Ohm's law gives the relation between a resistor, the current and voltage through that resistor:

$$I = \frac{V}{R}. \tag{13}$$

where:

I is the current through a resistor

V is the voltage across a resistor

R is the resistance of a resistor.

The current through a capacitor is given by:

$$I = C\frac{dV}{dt}. \tag{14}$$

where:

I is the current through a capacitor

C is the capacitance of a capacitor

$\frac{dV}{dt}$ is the rate of change of voltage across a capacitor.

Using these relations, differential equations were derived for each of the seven capacitors within the physiological model. These differential equations were written in state-space format and matrices A, B, C and D were obtained. Therefore, each value within those matrices can only be dependent on the values of the resistors and compliances given in the physiological model. The general state-space equations are given by:

$$\begin{aligned} \dot{x} &= Ax + Bu \\ y &= Cx + Du. \end{aligned} \tag{15}$$

where:

$\dot{x}$ is the rate of change of the state vector x

x is the state vector, containing the states of the 7 capacitors

u is the input vector, containing the 4 inputs of the model

y is the output vector, representing the intracranial pressure

A is the state matrix, representing the relation between x and $\dot{x}$

B is the input matrix, representing the relation between u and $\dot{x}$)

C is the output matrix, representing the relation between x and y)

D is the direct-transmission matrix, representing the relation between u and y).

In this case, the state vector x contains the voltages over each of the capacitors and y represents the ICP. The input vector u contains the four inputs of the model: the ABP, the superior sagittal sinus pressure, the CSF production rate and the cerebral ISF production rate. The derived matrices A, B, C and D can be found in the appendix. Using the ABP signal of each patients as an input signal, this model thus produces an 'ICP pulse'. By changing the values of the resistors as well as the compliances within this model, the ICP pulse produced by this model changes. The initial values of these parameters were set based on the results of Nassir et al. (2024) after the performed exhaustive model optimization, as detailed in table 3 of Nassir et al. (2024). The lower and upper bounds were defined as twice the standard deviation (SD) of each parameter. The SD value of each parameter is also provided in the previously referenced table of Nassir et al. (2024). Through minimisation of the sum of least squares between the measured ICP pulse of the

patient and the ICP pulse produced by the model, the optimal values for the resistors and compliances can be found. Several algorithms were used for this optimization done in Python, such as the Nelder-Mead algorithm and the Limited-memory Broyden–Fletcher–Goldfarb–Shanno with bounds (L-BFGS-B) algorithm [38, 39]. This resulted in a value of e.g. brain compliance for a patient.

4.6 Visualisation of all metrics

Each metric before, after as well as the difference over drainage is visualised over time in order to analyze changes. In order to compare the changes of each metric over consecutive drainagemoments between the analyzed patients, the obtained values before and after drainage were plotted as a five-period moving average during consecutive drainage moments in order to indicate the trend of all metrics over time. In order to visually compare 9 patients, the data of patients who survived the TBI are visualized together and the data of the patients who did not survive the TBI are visualized together. Furthermore, the y-axis scale for each parameter is standardized to enable clearer comparisons between patients who survived the TBI and those who did not. The choice for a five-period moving average is also based on future clinical use of certain metrics, which is explained in the future section of the discussion of this study. Next to this visualisation over time, the change of each metric over drainage for each patient is also visualised as boxplots for comparison.

5 Results

5.1 Patient characteristics

The characteristics of the patients available for this study can be found in table 2.

Table 2: *Characteristics of the patients available for this study. The number of drainage events consists of the drainage events before a secondary decompression (if present). ICP: Intracranial Pressure, EVD: External Ventricular drain.*

	Age	Gender	Time to ICP Insertion (hours post Trauma)	Time to EVD Insertion (hours post-ICP placement)	Duration of Simultaneous ICP and EVD (hours)	Number of drainage events	Secondary Decompression	Outcome
Patient 1	39	Male	2	117	87	55	No	Survivor
Patient 2	20	Male	6	82	180	58	No	Survivor
Patient 3	29	Male	5	11	104	48	Yes	Survivor
Patient 4	18	Female	1.5	28	454	226	No	Survivor
Patient 5	47	Female	13	15	102	98	No	Non-survivor
Patient 6	60	Male	4.5	66	257	123	No	Non-survivor
Patient 7	21	Male	1	8	28	21	Yes	Non-survivor
Patient 8	52	Male	3	269	110	18	No	Non-survivor
Patient 9	68	Female	5	139	168	38	No	Non-survivor

A total of 685 drainage events were annotated in 9 patients, ranging between 0 and 18 days after trauma. 79 drainage events were excluded, since these were not found in a time span of 30 minutes before and after the annotated timestamp and 72 events were excluded due to the presence of artefacts, resulting in 534 available drainage events.

5.2 Change in metrics over time

All figures can be found in the appendix. The metrics showing the most significant observable differences are outlined in this section. Interpretation of the results can be found in the discussion. The dP2/dP1 ratio shows observable differences, as can be seen in figure 9. This ratio represents the height of the second peak relative to the first peak in the ICP pulse. The ratio before and after the drainage events is represented by a dashed line and a dotted line, respectively. This ratio decreases in 8 patients over drainage, since the dotted line lies below the dashed line. This suggests that the second peak decreases over a single drainage event and/or the first peak increases over a single drainage event. In patient 9, indicated in brown, this ratio increases over drainage. This is caused by a larger decrease in dP1 than the decrease in dP2 over drainage, as can be seen in the appendix in figure 22, causing this ratio to increase.

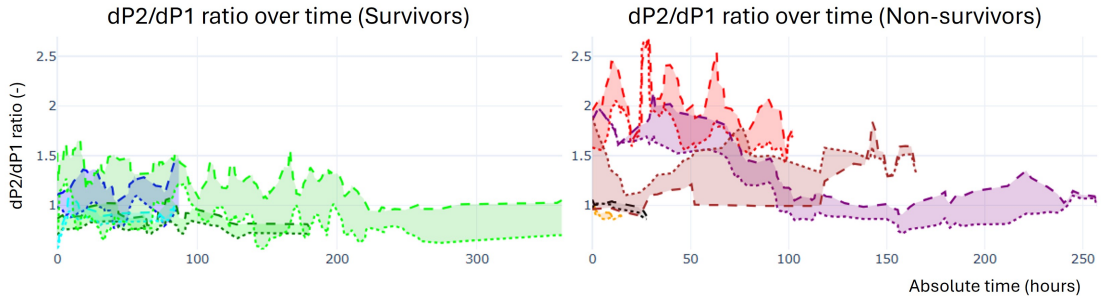

Figure 9: *In this figure, the dimensionless dP2/dP1 ratio is shown over time, with the ratio on the y-axis and absolute time after the first drainage event in hours on the x-axis. Data of TBI survivors, patient 1-4, is shown on the left panel as 'Group 1' and is indicated in blue, green, cyan and lime, respectively. Data of TBI non-survivors, patient 5-9, is shown on the right panel as 'Group 2' and is indicated in red, purple, orange, black and brown, respectively. The data is presented as a 5-period moving average to enhance visibility and facilitate the identification of potential trends over time. The dashed line represents the values before drainage, the dotted line represents values after drainage. The area between these lines is shaded for each patient to enhance visibility and quantify the extent of change over a single drainage event. TBI: Traumatic Brain Injury.*

The second ratio exhibiting observable differences, is the dP3/dP2 ratio (see figure 10). This ratio represents the height of the third peak relative to the first peak in the ICP pulse. This ratio increases in patient 2 (green), 3 (cyan), 4 (lime), 5 (red) and 9 (brown) over a single drainage event, since the dotted line lies above the dashed line. This can be observed more clearly in the boxplot of dP3/dP2, which is shown in the next section in figure 15. Since it is unlikely that the height of the third peak will increase over drainage, this increase must be caused by a decrease in the second peak over a single drainage event. In the other patients, the ratio decreases over a single drainage event, since the dotted line lies below the dashed line. Since it is unlikely that the height of the second peak will increase over drainage, this decrease must be caused by a decrease of the third peak over a single drainage event.

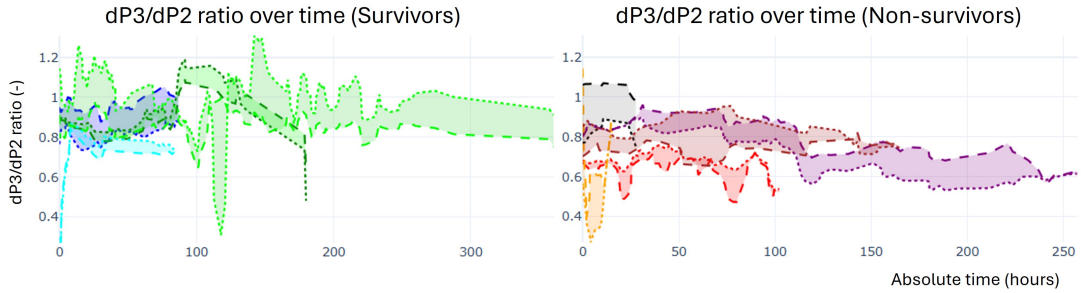

Figure 10: *In this figure, the dimensionless dP3/dP2 ratio is shown over time, with the ratio on the y-axis and absolute time after the first drainage event in hours on the x-axis. Data of TBI survivors, patient 1-4, is shown on the left panel as 'Group 1' and is indicated in blue, green, cyan and lime, respectively. Data of TBI non-survivors, patient 5-9, is shown on the right panel as 'Group 2' and is indicated in red, purple, orange, black and brown, respectively. The data is presented as a 5-period moving average to enhance visibility and facilitate the identification of potential trends over time. The dashed line represents the values before drainage, the dotted line represents values after drainage. The area between these lines is shaded for each patient to enhance visibility and quantify the extent of change over a single drainage event. TBI: Traumatic Brain Injury.*

Next to these ratio's, differences can be observed in the latency of the second (LP2) and third (LP3) peak (see figure 11). These latencies represent the latency of the second and third peak relative to the start of each ICP pulse. LP2 decreases over a single drainage event in the majority of the drainage events in all patients, with the exception of patient 4 (lime) and 6 (purple), since the dotted line lies below the dashed line in almost every case. This suggests that the latency of the second peak decreases over a single drainage event, indicating the second peak appears earlier in the ICP pulse. Since the dotted line lies above the dashed line in patient 4 and 6, the second peak appears later in the ICP pulse in these patients. LP3 increases over a single drainage event in the majority of the drainage events in all patients, with the exception of patient 5 (red) and 9 (brown), since the dotted line lies above the dashed line in almost every case. This suggests that the latency of the third peak increases over a single drainage event, indicating the third peak appears later in the ICP pulse. Since the dotted line lies below the dashed line in patient 5 and 9, the third peak appears earlier in the ICP pulse in these patients.

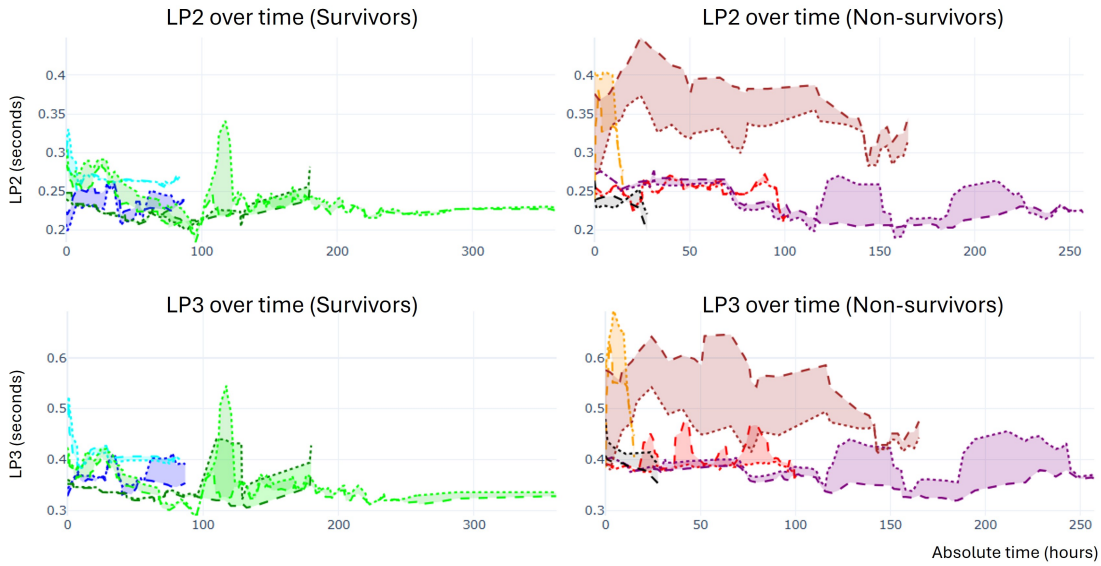

Figure 11: *In this figure, the latencies LP2 and LP3 are shown over time, with the latency in seconds on the y-axis and absolute time after the first drainage event in hours on the x-axis. Data of TBI survivors, patient 1-4, is shown on the left panel as 'Group 1' and is indicated in blue, green, cyan and lime, respectively. Data of TBI non-survivors, patient 5-9, is shown on the right panel as 'Group 2' and is indicated in red, purple, orange, black and brown, respectively. The data is presented as a 5-period moving average to enhance visibility and facilitate the identification of potential trends over time. The dashed line represents the values before drainage, the dotted line represents values after drainage. The area between these lines is shaded for each patient to enhance visibility and quantify the extent of change over a single drainage event. TBI: Traumatic Brain Injury.*

Due to the observed differences in LP2 and LP3, differences can also be observed in the latency between P3 and P1 (LP3-LP1) as well as between P3 and P2 (LP3-LP2) as can be seen in figure 12. Both latency differences increase over a single drainage event in the majority of the drainage events in all patients, with the exception of patient 5 (red) and 9 (brown), since the dotted line lies above the dashed line in almost every case. This suggests that both latency differences increase over a single drainage event, indicating an increasing distance between the first and third peak as well as between the second and third peak in the ICP pulse over drainage. Since the dotted line lies below the dashed line in patient 5 and 9, this suggests a decreasing distance over a single drainage event. This indicates a decreasing distance between the first and third peak as well as between the second and third peak in the ICP pulse over drainage.

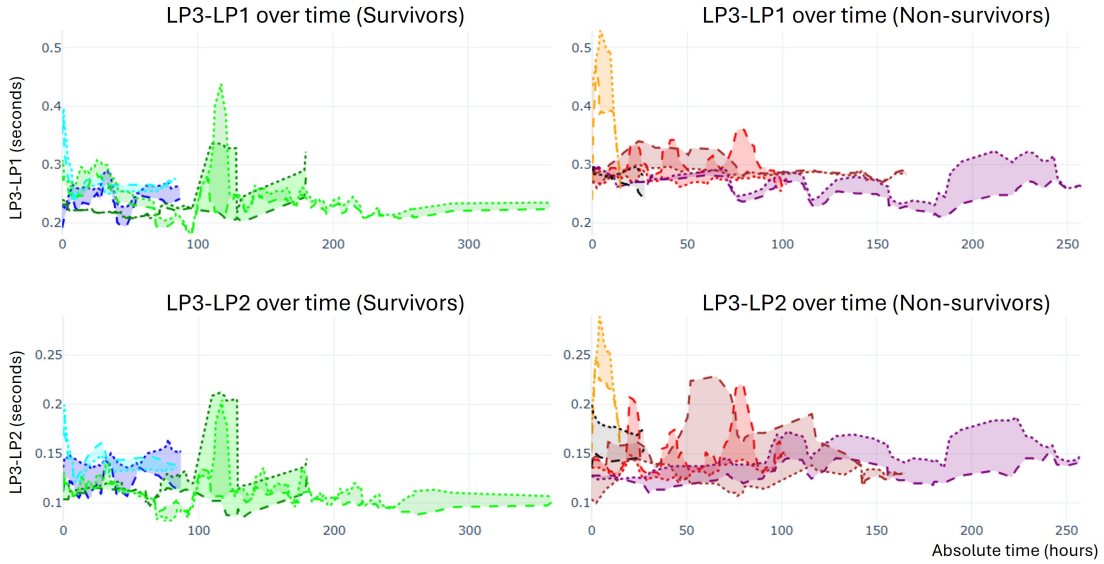

Figure 12: *In this figure, the latency differences LP3-LP1 and LP3-LP2 are shown over time, with the latency in seconds on the y-axis and absolute time after the first drainage event in hours on the x-axis. Data of TBI survivors, patient 1-4, is shown on the left panel as 'Group 1' and is indicated in blue, green, cyan and lime, respectively. Data of TBI non-survivors, patient 5-9, is shown on the right panel as 'Group 2' and is indicated in red, purple, orange, black and brown, respectively. The data is presented as a 5-period moving average to enhance visibility and facilitate the identification of potential trends over time. The dashed line represents the values before drainage, the dotted line represents values after drainage. The area between these lines is shaded for each patient to enhance visibility and quantify the extent of change over a single drainage event. TBI: Traumatic Brain Injury.*

Regarding the weighted-ICP, a decrease over a single drainage event is observed in most of the drainage events in patient 1 (blue), 3 (cyan), 5 (red) and 9 (brown) since the dotted line lies below the dashed line in almost every case (see figure 13. This suggests that the weighted-ICP decreases over a single drainage event. In the other patients, the dotted line lies above the dashed line in almost every case. This suggests that the weighted-ICP increases over a single drainage event in these patients.

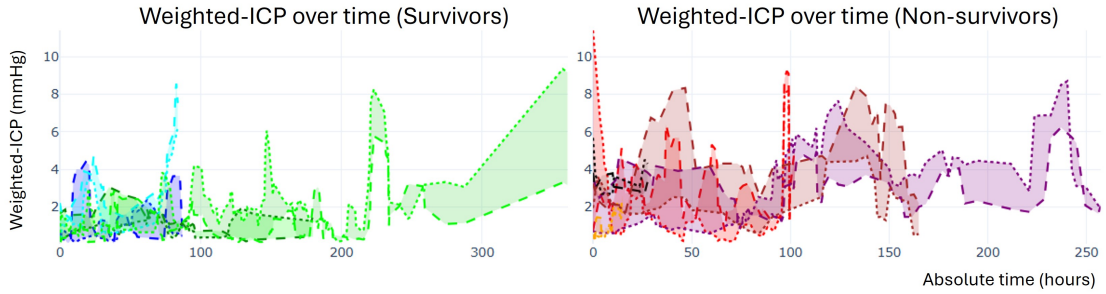

Figure 13: *In this figure, the weighted−ICP is shown over time, with the weighted−ICP in mmHg on the y-axis and absolute time after the first drainage event in hours on the x-axis. Data of TBI survivors, patient 1-4, is shown on the left panel as 'Group 1' and is indicated in blue, green, cyan and lime, respectively. Data of TBI non-survivors, patient 5-9, is shown on the right panel as 'Group 2' and is indicated in red, purple, orange, black and brown, respectively. The data is presented as a 5-period moving average to enhance visibility and facilitate the identification of potential trends over time. The dashed line represents the values before drainage, the dotted line represents values after drainage. The area between these lines is shaded for each patient to enhance visibility and quantify the extent of change over a single drainage event. ICP: Intracranial Pressure, TBI: Traumatic Brain Injury.*

Similar differences can be observed in the RAP-index, see figure 14. A decrease over a single drainage event is observed in most of the drainage events in all patients, with the exception of patient 5 (red), 9 (brown) and the first half of the drainage treatment of patient 6 (purple), since the dotted line lies below the dashed line in almost every case. This suggests that the RAP-index decreases over a single drainage event. In patient 5, 9 and in the second half of the drainage treatment of patient 6 (purple), the dotted line lies above the dashed line in almost every case. This suggests that the RAP-index increases over a single drainage event in these patients.

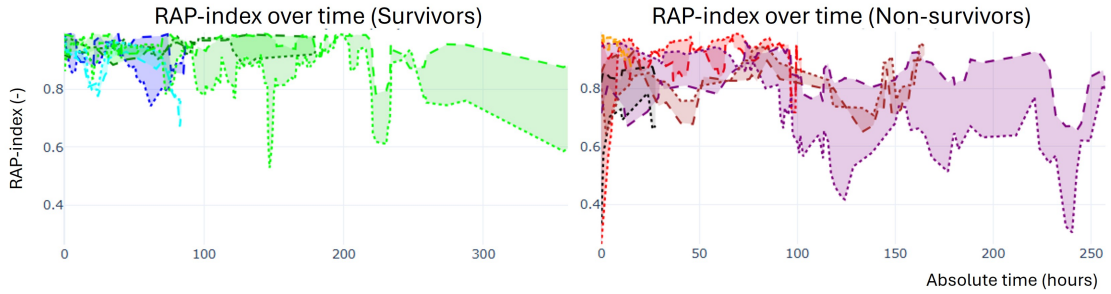

Figure 14: *In this figure, the dimensionless RAP−index is shown over time, with the RAP−index on the y-axis and absolute time after the first drainage event in hours on the x-axis. Data of TBI survivors, patient 1-4, is shown on the left panel as 'Group 1' and is indicated in blue, green, cyan and lime, respectively. Data of TBI non-survivors, patient 5-9, is shown on the right panel as 'Group 2' and is indicated in red, purple, orange, black and brown, respectively. The data is presented as a 5-period moving average to enhance visibility and facilitate the identification of potential trends over time. The dashed line represents the values before drainage, the dotted line represents values after drainage. The area between these lines is shaded for each patient to enhance visibility and quantify the extent of change over a single drainage event. TBI: Traumatic Brain Injury.*

5.3 Change in metrics over all drainage events

In order to visualise the difference of each metric over drainage, a boxplot is made for all patients. This difference over drainage is calculated as shown in equation 8 on page 21. All boxplots can be found in the appendix.
Again, the dP3/dP2 ratio shows observable differences as can be seen in figure 15. Patient 2,3,4,5 and 9 show a positive change over a single drainage event, indicating a increasing dP3/dP2 ratio over drainage as is observed in figure 10. This suggests a decreasing height of P2 over a drainage event in these patients. Patient 1,6,7 and 8 show a negative change over a single drainage event, indicating a decreasing dP3/dP2 ratio over drainage. This suggests a decreasing height of P3 over a drainage event in these patients.

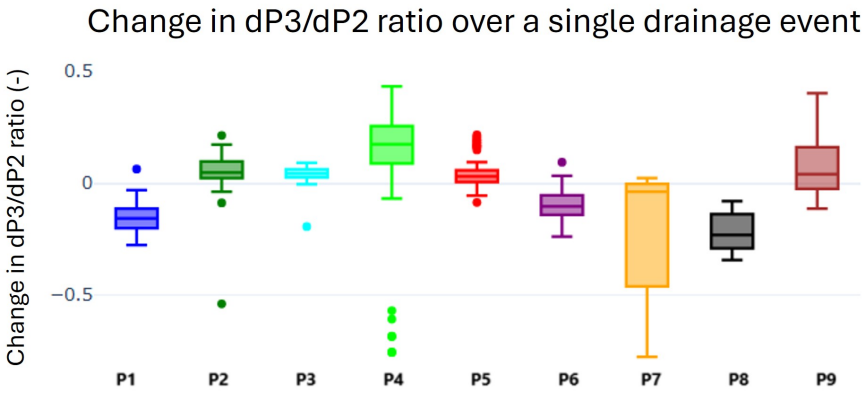

Figure 15: *In this figure, the change in the dimensionless dP3/dP2 ratio over a single drainage event is shown for each patient, indicated by P1-P9. Data of TBI survivors, patient 1-4, is indicated in blue, green, cyan and lime, respectively. Data of TBI non-survivors, patient 5-9, is indicated in red, purple, orange, black and brown, respectively. The data is presented as a boxplot. The edges of the boxes indicate the 25th (Q1) and 75th (Q3) percentiles, whereas whiskers give the minimum and maximum values. Outliers are presented as single dots outside these whiskers. TBI: Traumatic Brain Injury.*

5.4 Change in metrics in relation with accompanying ICP change

In order to observe the data in another perspective, the change of each metric over a single drainage event in relation with the change in ICP of a single drainage event is visualized. All figures can be found in the appendix.
The first observable difference can be found in the curvature of the first peak of the ICP pulse, as shown in figure 16. Patients in group 1 show in most cases a relative large positive change in the curvature in relation with the accompanying ICP difference. This suggests the curvature of the first peak increases over a single drainage event, indicating a more distinct first peak in the ICP pulse. Patients in group 2 however, show also negative changes in the curvature. This suggests the curvature of the first peak decreases over a single drainage event, indicating a less distinct first peak in the ICP pulse.

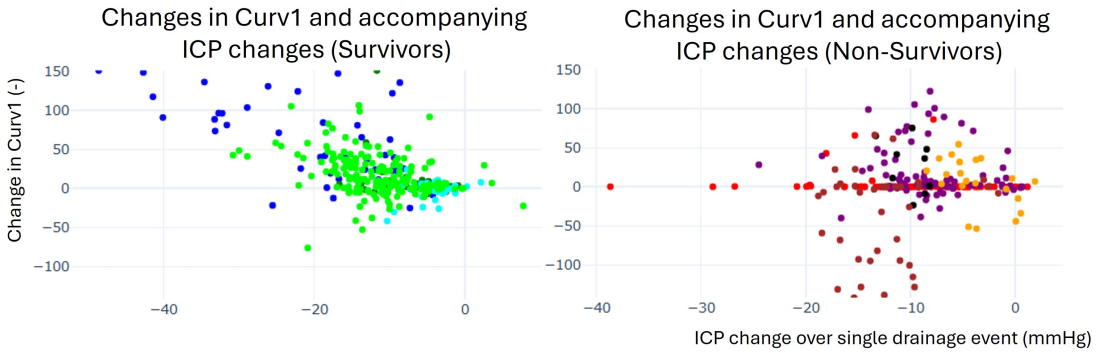

Figure 16: *In this figure, the change in the curvature of the first peak of the ICP pulse is shown on the y-axis with the accompanying change in ICP in mmHg on the x-axis over a single drainage event. Data of TBI survivors, patient 1-4, is shown on the left panel as 'Group 1' and is indicated in blue, green, cyan and lime, respectively. Data of TBI non-survivors, patient 5-9, is shown on the right panel as 'Group 2' and is indicated in red, purple, orange, black and brown, respectively. ICP: Intracranial Pressure, TBI: Traumatic Brain Injury.*

The HHC metric also shows observable differences, as can be seen in figure 17. Patients in group 1 show in most cases a negative change in HHC in relation with the accompanying ICP difference. This suggests that the HHC decreases over a single drainage event in these patients. However, patients in group 2 exhibit a positive change in HHC in most cases, indicating an increase in HHC over a single drainage event.

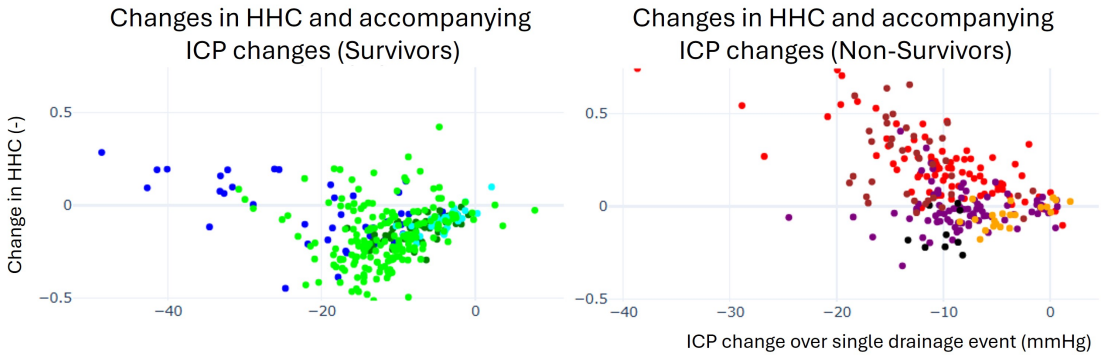

Figure 17: *In this figure, the change in the HHC is shown on the y-axis with the accompanying change in ICP in mmHg on the x-axis over a single drainage event. Data of TBI survivors, patient 1-4, is shown on the left panel as 'Group 1' and is indicated in blue, green, cyan and lime, respectively. Data of TBI non-survivors, patient 5-9, is shown on the right panel as 'Group 2' and is indicated in red, purple, orange, black and brown, respectively. HHC: Higher Harmonic Centroid, ICP: Intracranial Pressure, TBI: Traumatic Brain Injury.*

Next to the HHC metric, the HFC-power metric also shows observable differences as can be seen in figure 18. Patients in group 1 show larger as well as more frequent negative changes in HFC-power in relation with the accompanying ICP difference than patients in group 2. This suggests that the HFC-power decrease over a single drainage event is larger as well as more frequent in

these patients compared to the patients in group 2.

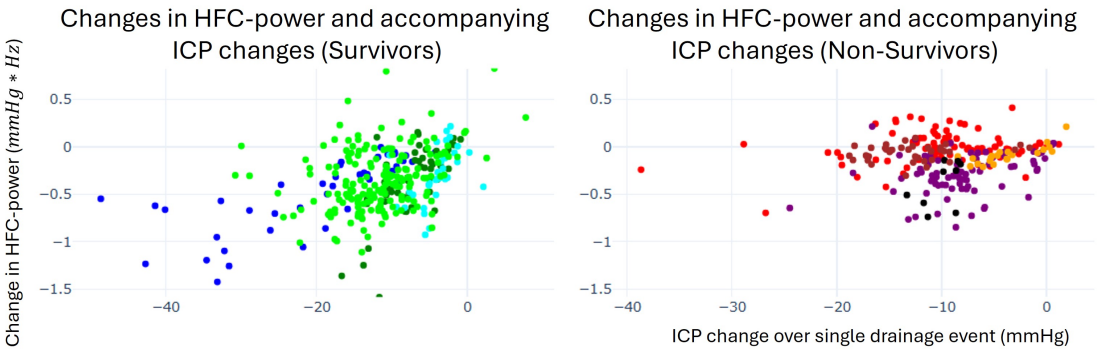

Figure 18: *In this figure, the change in the HFC-power in $mmHg * Hz$ is shown on the y-axis with the accompanying change in ICP in mmHg on the x-axis over a single drainage event. Data of TBI survivors, patient 1-4, is shown on the left panel as 'Group 1' and is indicated in blue, green, cyan and lime, respectively. Data of TBI non-survivors, patient 5-9, is shown on the right panel as 'Group 2' and is indicated in red, purple, orange, black and brown, respectively. HFC: Higher Frequency Centroid, ICP: Intracranial Pressure, TBI: Traumatic Brain Injury.*

5.5 Viscoelastic model

After deriving the 7 differential equations for each capacitor in the model of figure 7, these differential equations were written in a state-space representation. In appendix 8 this representation can be found. In order to verify the stability of the model, a zero-input as well as the ABP-input is given to the model. In both scenarios, the stability of each differential equation (state space) is verified through a visualisation over time as can be seen in figure 19. After this verification, the model runs to find the optimal parameters to minimize the SSD between the measured ICP signal and the simulated ICP signal. The Limited-memory Broyden–Fletcher–Goldfarb–Shanno with bounds (L-BFGS-B) algorithm had the best results, based on duration of the optimization as well as the result of the simulated ICP waveform. Although a correct scaling of the ABP wave towards the ICP signal is obtained, the model has difficulty in introducing the second characteristic peak within the ICP pulse as can be seen in figure 20.

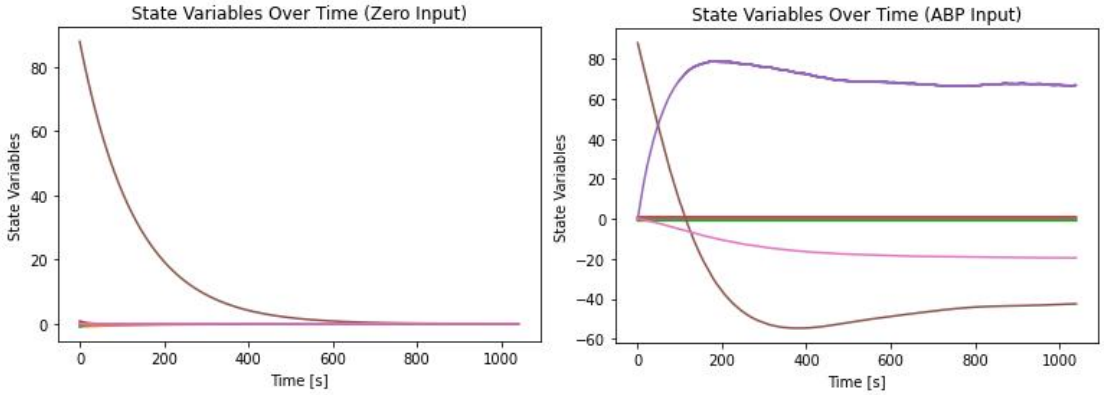

Figure 19: *Convergence of the state-space model with initial values for all parameters and either a zero input or ABP input. The evolution of the seven states is shown in different colours to illustrate the behaviour of the viscoelastic model over time*

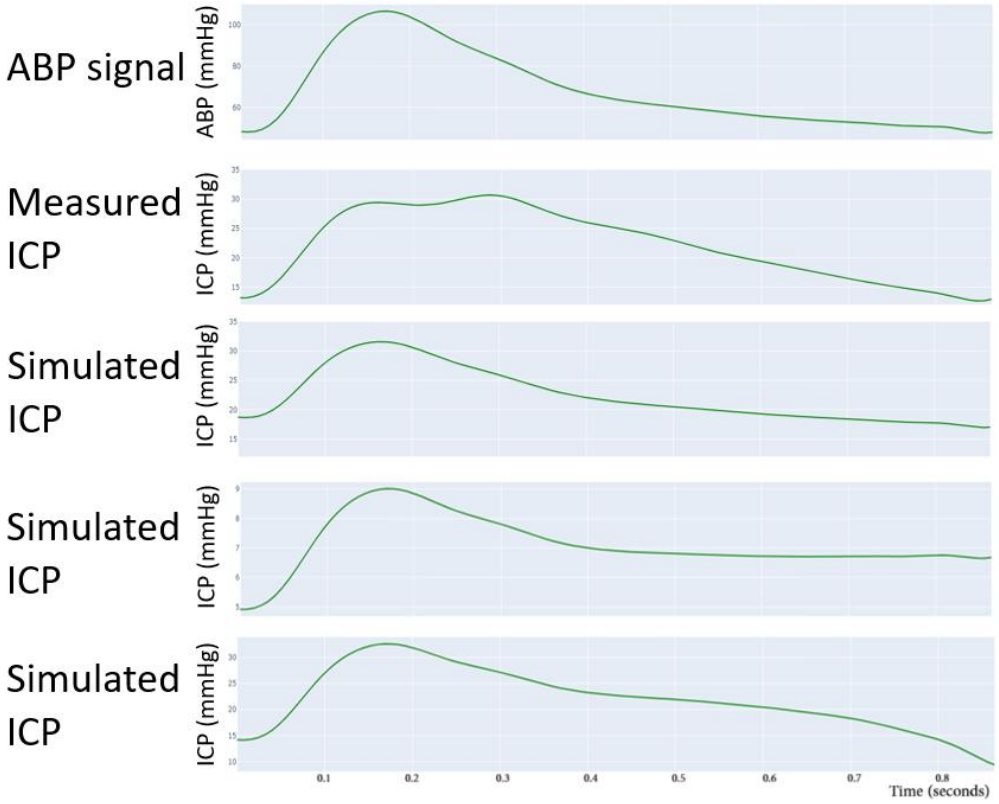

Figure 20: *The first panel shows a single ABP pulse of a patient. The accompanying ICP signal measured in this patient is shown in panel 2. In panel 3-5 several simulated ICP pulses can be seen. Differences between simulated ICP pulses are caused by manual changing several parameters.*

5.6 Brain compliance during precisely measured drainage events

Patient 9 was the only patient admitted to the ICU in the RadboudUMC during this study. After drainage event 1−6, the drained volume through the EVD was measured exactly. Therefore, an exact calculation of the brain compliance was possible. The results are shown in figure 21 together with the RAP-index of this patient for comparison. Most compliance values can be found in the range of 0.2−0.6 ml/mmHg.

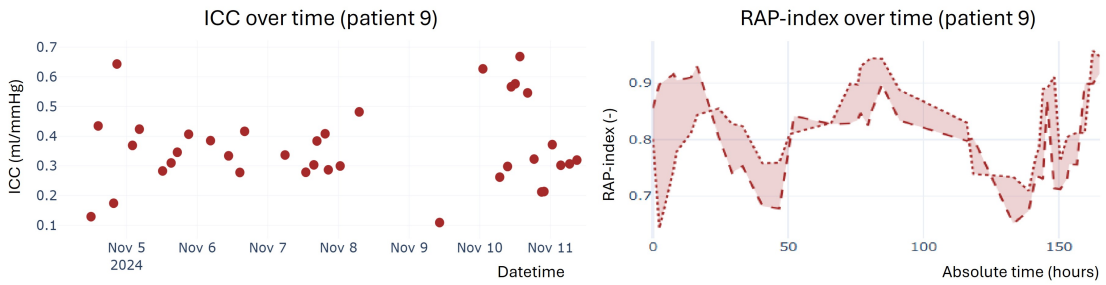

Figure 21: *In this figure, the brain compliance of patient 9 is shown over time on the left, with the compliance in ml/mmHg on the y-axis and the date−time on the x-axis. In drainage event 1−6, the brain compliance was calculated based on approximate measurements of drained volumes. Starting from drainage event 7, the drained volume through the EVD was measured exactly. On the right, the RAP-index of patient 9 is shown, with the RAP−index on the y-axis and absolute time after the first drainage event in hours on the x-axis. The data is presented as a 5-period moving average to enhance visibility and facilitate the identification of potential trends over time. The dashed line represents the values before drainage, the dotted line represents values after drainage. The area between these lines is shaded to enhance visibility and quantify the extent of change over a single drainage event. EVD: external ventricular drain.*

6 Discussion

In this this research 534 drainage events were identified in nine patients and for each drainage moment several metrics were calculated before and after drainage. Through waveform morphology analysis, an overview of the clinical significance of each method in analyzing the ICC in TBI patients on the ICU can be given. Several metrics showed differences over time as well as differences in mortality, suggesting a clinical significance of these metrics regarding the clinical outcome of a TBI patient. These observed differences are discussed in this section and compared to the 'golden standard' RAP-index, in order to conclude this study with a recommendation for the metric which holds the most promising clinical utility in analyzing the ICC in TBI patients on the ICU.

6.1 Interpretation of the results

In the analysis of all metrics over time, the dP2/dP1 ratio, dP3/dP2 ratio, LP2, LP3, LP3-LP1, LP3-LP2, weighted ICP and the RAP−index showed substantial changes. In addition to these metrics over time, the boxplot of all drainage events of dP3/dP2 also showed substantial changes between patients. In relation with the accompanying ICP change over a drainage event, the Curv1, HHC as well as the HFC-power metric showed observable differences.

The dP2/dP1 ratio remains stable around a ratio of 1 before and after drainage for survivors, suggesting a relative consistent height difference over time. This indicates that the brain compliance remains relatively constant over time in TBI survivors. Non-survivors show a slight decreasing or increasing trend over time. A decreasing trend suggests that either the height of the second peak decreases and/or the height of the first peak increases over time. As can be seen in figure 22 in appendix A, dP2 indeed decreases in all patients over drainage. This suggests that the brain compliance improves over time. Conversely, a increasing trend suggests a deterioration in brain compliance over time. One can see that the non-survivors start with a worse dP2/dP1 ratio compared to survivors (the ratio is almost 2x higher). This indicates that the height of the second peak is 2x higher than the first peak in non-survivors compared to survivors, thus indicating a less compliant brain for non-survivors. Since P2<P1 in a normal state, a ratio of preferable <1 indicates a compliant brain. It can be seen that the data of the survivors lies in this range, whereas the data of the non-survivors lies in a higher range. Patient 6, indicated in purple, reaches a dP2/dP1 ratio of around 1 after 100 hours since the first drainage event. This suggest that the brain compliance has improved in this patient over time. Patient 9 however, shows a deterioration in brain compliance due to the slight increasing trend over time.

The observed changes over drainage in the dP3/dP2 ratio, an increasing as well as decreasing ratio over a single drainage event, both indicate that the compliance improves over drainage due to either a decreased height of the second or third peak over drainage. As can be seen in figure 22 in appendix A, both peaks decrease in all patients over drainage. The survivors exhibit a relative stable trend over time at a dP3/dP2 ratio around 0.8-1. This suggests that the relative height difference between the third and second peak remains consistent over time, indicating that the brain compliance remains relatively constant over time. Non-survivors either show a relative stable trend over time at a dP3/dP2 ratio around 0.6-0.8 or a declining trend over time towards this 0.6-0.8 ratio. This declining trend suggests that the third peak shows a relatively greater decrease over time compared to the second peak, suggesting that the brain compliance improves slightly over time. However, the 0.6-0.8 ratio in non-survivors compared to the 0.8-1.0 ratio in survivors, indicates that p2 and p3 are relatively constant in survivors

whereas p3 is considerably lower than p2 in non-survivors. A possible explanation for this difference in ratio could be that due to a less compliant brain in non-survivors, the second peak dominates the ICP pulse and thus causes a relative suppression of the third peak in the ICP pulse.

Regarding the latency of the second and third peak in the ICP pulse, all patients show a stable or a slight decreasing trend over time in both latencies. A stable trend suggests that the appearance of the second or third peak in the ICP pulse remains consistent over time, indicating a brain compliance which remains unchanged over time. However, a slight decreasing trend suggests an earlier appearance of the second or third peak in the ICP pulse over time. Since the second and third peak will appear later in an ICP pulse in a less compliant brain, this decreasing trend suggests that the brain compliance improves over time in these patients. Comparing the survivors with the non-survivors, it appears that LP2 is larger at the first drainage event and/or remains larger over time in non-survivors compared to survivors. This means, that the second peak appears later in the ICP pulse in non-survivors for a longer period of time compared to survivors. Over time, this larger latency decreases in non-survivors to a value of around 0.20-0.25 seconds. It can be seen that the survivors reach this value earlier after the first drainage event than non-survivors. Similar differences can be observed at LP3, which also appears to be larger at the first drainage event and/or remains larger over time in non-survivors compared to survivors. This means, that the third peak appears later in the ICP pulse in non-survivors for a longer period of time compared to survivors. Over time, this larger latency decreases in non-survivors to a value of around 0.4 seconds. It can be seen that the survivors reach this value (or a lower value) earlier after the first drainage event and show a stable/decreasing trend over time to a value of around 0.35 seconds.

Similar to LP2 and LP3, all patients show a stable or slight decreasing trend over time in both latency differences LP3-LP1 and LP3-LP2. A stable trend suggests that the distance between those peaks in the ICP pulse remains consistent over time, indicating a brain compliance which remains unchanged over time. However, a slight decreasing trend suggests a decreasing distance between the first and third peak as well as between the second and third peak in the ICP pulse over time. In a less compliant brain, the peaks of the ICP pulse can be merged together (see figure 2E). This causes a larger distance between the peaks. Therefore, if the peaks become more distinct during drainage, the distances between the peaks decreases slightly. Thus, the observed slight decreasing trend in these latency differences indicates that the brain compliance slightly improves over time in these patients. Furthermore, differences can be observed between survivors and non-survivors. Both the LP3-LP1 latency and the LP3-LP2 latency appear to be larger at the first drainage event and/or remains larger over time in non-survivors compared to survivors. This means that the distances between those peaks in the ICP pulse are larger in non-survivors for a longer period of time compared to survivors, indicating possible merged peaks in the ICP pulse of non-survivors and thus a less compliant brain than the survivors.

The observed differences in weighted$-$ICP are related to the observed differences in the RAP-index, since the weighted-ICP depends on the value of the RAP$-$index (see equation 2). The weighted$-$ICP decreases over a single drainage event in patient 1, 3, 5 and 9, which is caused by a lower ICP after the drainage event and/or a higher RAP$-$index. Since the RAP$-$index is a Pearson correlation coefficient, a higher RAP$-$index indicates that there is a stronger positive correlation between the mean ICP and the amplitude of each ICP pulse. A stronger positive correlation could perhaps indicate a relatively compliant brain, since a relative high RAP$-$index close to 1 could reflect a state where the brain still has a relatively predictable, although limited, compensatory capacity. The brain might still be able to respond in a relative consistent

manner, where increases in mean ICP are accompanied by proportional increases in amplitude, suggesting a reasonable compliant brain. Therefore, the decrease in weighted−ICP over a single drainage event in these patients could suggest an improving brain compliance over drainage. The observed increase of the weighted−ICP over a single drainage event in the other patients, is caused by a lower RAP−index since the ICP after drainage can not be higher than before drainage. A lower RAP−index indicates a weaker positive correlation between the mean ICP and amplitude of the ICP pulse. This could perhaps indicate a non compliant brain due to more unstable or non-linear brain compliance, inducing 'erratic' changes in amplitude of the ICP pulse in response to changes in the mean ICP. Therefore, the increase in weighted−ICP over a single drainage event in these patients could suggest a deteriorating brain compliance over drainage. All patients show a relative stable trend of the weighted−ICP over time, indicating a brain compliance which remains unchanged over time. Although, there is an increase at the end of the drainage treatment in patient 4 (lime). This could indicate a decreasing brain compliance in this patient. However, since this patient survived the TBI, this observation should be interpreted with caution. Furthermore, survivors show a relative low weighted−ICP value around 2mmHg during drainage treatment, whereas non-survivors show a larger weighted−ICP value around 4mmHg during drainage treatment. This larger weighted−ICP value could indicate that non-survivors have a less compliant brain compared to the survivors, due to a lower RAP−index value.

The RAP−index decreases over a single drainage event in most of the drainage events in all patients, which could indicate a deteriorating brain compliance over drainage. The increase over a single drainage event in patient 5, 9 and the first half of the drainage treatment of patient 6, could suggest an improving brain compliance over drainage. All patients show a relative stable trend of the RAP−index over time, indicating a brain compliance which remains unchanged over time. Although, there is decrease at the end of the drainage treatment in patient 4 (lime). This could indicate a decreasing brain compliance in this patient. However, since this patient survived the TBI, this observation should be interpreted with caution. Furthermore, survivors show a RAP−index close to 1 whereas non-survivors show a slightly smaller RAP−index value of around 0.8. Especially in patient 6 (purple), the RAP−index value after drainage is significantly lower than before drainage. This slightly lower RAP−index value in non-survivors could thus indicate that non-survivors have a less-compliant brain compared to the survivors.

Next to these observable changes over time, the boxplot of the dP3/dP2 ratio of each patient showed a relative large observable difference over a single drainage event. A negative difference, suggesting a decreasing height of P3 over drainage, as well as a positive difference, suggesting a decreasing height of P2 over drainage, both indicate an improvement in brain compliance. However, a decreasing height of P2 is argued to be superior as a metric for an improvement in compliance. Hence, a positive change in dP3/dP2 ratio over a single drainage event could be considered as more effective than a negative change. Therefore, this could be a metric for the clinical physician which could immediately indicate a more effective drainage after a single drainage event if the dP3/dP2 ratio has a positive change. Due to this immediate ability to check the drainage event, this metric has a high clinical utility.

The curvature of the first peak in the ICP pulse, Curv1, showed observable differences in relation with the accompanying ICP change of a single drainage event. Survivors exhibit in most cases a larger positive change in Curv1 than non-survivors, which show more negative as well as smaller positive changes in Curv1 over a single drainage event. This indicates that survivors show a more distinct first peak in the ICP pulse after a drainage event compared to non-survivors. Furthermore, the observed negative changes over a drainage event in non-survivors suggest that

these patients are inclined to demonstrate merged peaks in the ICP pulse after a drainage event. Since survivors show more frequent and larger curvature changes over a single drainage event, non-survivors show ICP pulses after drainage characterized by a less distinct first peak and thus a less compliant brain.

Next to the curvature, the HHC metric showed observable differences in relation with the accompanying ICP change of a single drainage event. Survivors show a decrease in HHC over drainage in most drainage events, whereas non-survivors show an increase in HHC over drainage. Since an increase in HHC could be interpreted as an increase in the distortion of the ICP pulse (irrespective of the heart rate), this observed increase in HHC in non-survivors suggests that these patients exhibit a more distorted ICP pulse after drainage and thus a reduced brain compliance. Furthermore, since survivors exhibit a decrease in HHC, the ICP pulse is inclined to show improvement over drainage and thus an improvement in brain compliance in survivors. Next to the positive and negative difference over a single drainage event, a relative stable or subtle increasing trend could be observed in the survivors. This slight increasing trend suggests that a greater ICP difference over drainage is associated with less distortion of the ICP pulse after drainage, indicating an improved brain compliance. However, non-survivors exhibit a slight decreasing trend. This suggests that a greater ICP difference over drainage is associated with more distortion of the ICP pulse after drainage, indicating a reduced brain compliance. Although these multiple observable differences, the clinical utility of the HHC metric is limited due to the multiple conditions which must be met for an effective application. First of al, the ICP signal needs to be analyzed in the frequency domain. Secondly, several drainage events are needed before a trend could be observed. Therefore, the HHC metric cannot be implemented directly in the clinical setting on the ICU.

In addition to the HHC metric, the HFC-power metric also shows observable differences in relation with the accompanying ICP change of a single drainage event. Survivors show a larger and more frequent decrease in HFC-power over drainage in most drainage events. The HFC-power metric is the adjusted HFC metric (see equation 5). The HFC-power metric has a quadratic spectral amplitude, therefore giving 'weight' to this metric and thus results in an 'intensity' metric. The HFC-power metric is thus a measure of the intensity−weighted average frequency within 4−15Hz. A decrease in HFC-power could therefore be interpreted as a diminished presence of higher frequency components in the ICP pulse. Since this decrease is larger and more frequently observed in TBI survivors, this suggests that after a drainage event less higher frequency components are present in the ICP pulse compared to TBI non-survivors. This could indicate the ICP pulse is more stable after drainage in TBI survivors and thus unstable in TBI non-survivors, suggesting a more compliant brain in survivors after a drainage event. Next to this difference between survivors and non-survivors over a drainage event, a subtle increasing trend could be observed in TBI survivors. This slight increasing trend suggests that a greater ICP difference over drainage is associated with a more diminished presence of higher frequencies in the ICP pulse after drainage, indicating a more stable ICP pulse and thus an improved brain compliance. However, non-survivors exhibit a relatively stable trend. Furthermore, this stable trend occurs within a smaller magnitude of negative changes. This suggests that higher frequency components are more prevalent in the ICP pulse after drainage, indicating an unstable ICP pulse and thus a reduced brain compliance. However, for the same reasons as with the HHC metric, the clinical utility of the HFC-power metric is limited.

Finally, brain compliance in patient 9 was calculated by accurately measuring the drained volumes through the EVD. A relatively stable trend around 0.3−0.4 ml/mmHg over time can be

observed, with a potential slight decreasing trend. This suggests that brain compliance either remained relatively stable throughout the drainage events or decreased slightly. Since patient 9 did not survive the TBI, the slight decreasing trend appears to align with the clinical outcome of this patient. However, at the end of the drainage treatment large compliance values introduce some uncertainty in this statement. Furthermore, since the RAP−index for this patient is also relative stable between 0.7−0.9 over time, neither metric provides additional information compared to the other. Nonetheless, the RAP−index is an indirect measure of brain compliance and exhibits minimal variation between the analyzed patients. Accurately measuring drained volumes in a larger cohort of patients could potentially show differences, thereby endorsing this method over the RAP−index.

To provide a comparative analysis of all metrics, table 3 summarizes the clinical relevance and predictive power, as well as the comparison with the RAP−index of each metric. The strengths and weaknesses of each metric are thus highlighted in this table, thereby assisting in the identification of the most promising metrics for future clinical utility.

Table 3: *Comparative Analysis regarding the clinical relevance, predictive power and comparison with the RAP−index of analyzed metrics in this study.*

Metric	Clinical Relevance	Predictive Power	Comparison with RAP−index
dP2/dP1 ratio	A higher ratio indicates a less compliant brain	Non-survivors exhibit ratio of 2 compared to a ratio of 1 in survivors at start of drainage treatment	Outperforms RAP−index during whole drainage treatment, especially at the start
dP3/dP2 ratio	Both a decreasing or increasing trend indicate improvement of the brain compliance	Non-survivors exhibit a stable ratio of around 0.6-0.8 (or a decreasing trend towards this ratio) compared to a ratio of 0.8-1.0 in survivors during drainage treatment.	Outperforms RAP−index over whole drainage treatment. Also outperforms RAP−index due to the immediate observable effect after a single drainage event
LP2	Lower LP2 indicates earlier appearance of P2 in the ICP pulse and thus a more compliant brain	Earlier appearance of LP2 <= 0.25 seconds could indicate a relative compliant brain and a possible TBI survivor	Outperforms RAP−index over whole drainage treatment
LP3	Lower LP3 indicates earlier appearance of P3 in the ICP pulse and thus a more compliant brain	Earlier appearance of LP3 <= 0.4 seconds could indicate a relative compliant brain and a possible TBI survivor	Outperforms RAP−index over whole drainage treatment
LP3 - LP1	Lower LP3-LP1 indicates less time between P3 and P1 in the ICP pulse, suggesting a more compliant brain.	Earlier appearance of a decrease in LP3-LP1 could indicate a relative compliant brain and a possible TBI survivor	Outperforms RAP−index over whole drainage treatment
LP3 - LP2	Lower LP3-LP2 indicates less time between P3 and P2 in the ICP pulse, suggesting a more compliant brain.	Earlier appearance of a decrease in LP3-LP2 could indicate a relative compliant brain and a possible TBI survivor	Outperforms RAP−index over whole drainage treatment
Weighted ICP	Increase in weighted ICP indicates a decrease in brain compliance	A weighted ICP > 2 mmHg or an increasing trend over time could indicate a relative non-compliant brain and a possible TBI non-survivor	Outperforms RAP−index over whole drainage treatment
Curv1	Increase over single drainage event indicates an effective drainage and thus a decrease in brain compliance	Frequent increase over drainage events indicates an effective drainage and a possible TBI survivor	Outperforms RAP−index, due to the immediate observable effect after a single drainage event
HHC	Decrease over single drainage event indicates a less distorted ICP pulse and thus an improved brain compliance	Decrease over single drainage event indicates an effective drainage and a possible TBI survivor	Although observable differences, frequency analysis is needed
HFC-power	Decrease over single drainage event indicates a more stable ICP pulse and thus an improved brain compliance	Decrease over single drainage event indicates an effective drainage and a possible TBI survivor	Although observable differences, frequency analysis is needed
RAP−index	Golden standard in this study. A decrease in RAP−index over time could indicate a decrease in brain compliance	A decreasing trend over time indicates a less compliant brain and a possible TBI non-survivor	Standard benchmark for comparison in this study

6.2 Viscoelastic Model

The current model has the ability to scale the ABP waveform to the range of the ICP pulse, but has some difficulties in for instance introducing the second characteristic peak in the ICP pulse. Therefore, the current version of the model has no clinical significance and needs further adjustments. The major reason for the current incorrect functioning of the model, is due to time limitations. Challenges in generating an ICP pulse which closely resembled the measured ICP pulse of the patient, were caused by the parameter optimization. Through minimisation of the sum of least squares between the measured ICP pulse of the patient and the ICP pulse produced by the model, the optimal values for the resistors and compliances were found. However, the model required an extended runtime, which resulted in no solution for the optimal parameters. Therefore, a minimal SSD value was set as a target for the model to achieve. While running the model for a longer period might have been beneficial, after running the model for at least a full day, it was decided to set a minimal SSD threshold to obtain results. Furthermore, due to time limitations, a detailed analysis regarding the difference between several parameter optimization algorithms was not conducted. It may not be possible to optimize all parameters individually, since resistors and capacitors are interrelated, which poses significant challenges for optimization. Nevertheless, Nassir et al. (2024) did successfully manage to address this issue, and a recent algorithm has been proposed to tackle the multi-objective resistance-capacitance optimization problem [40]. This suggests that parameter optimization is achievable for this viscoelastic model. If existing challenges are addressed, this model could provide immediate insights for clinical physicians regarding the ICC in TBI patients on the ICU.

6.3 Limitations

There are several remarks regarding this study. First, it should be noted that the threshold value of pathological IH at 20mmHg is more a guideline than a rigid cut-off value, e.g. the recent guidelines of the Brain Trauma Foundation moved this threshold to 22mmHg based on just one single-centre, retrospective study [8]. Apart from the fact that this is more a guideline than a rigid cut-off value, this is an oversimplification for all TBI patients. The association between IH and clinical outcome is established, but this does not translate towards a single treatment threshold [9]. After severe TBI, the brain physiology cannot be simplified to a threshold-based management strategy due to the complex interaction between ICP, cerebral blood flow, brain metabolism, feedback systems of neurovascular (un)coupling, cerebral auto-regulation and CO_2 reactivity [9]. Therefore, in addition to ICP pulse morphology, other parameters such as cerebral blood flow might offer additional or even superior insights for assessing the ICC of TBI patients in the ICU.

In this study, nine patients were analyzed and differences were observed in 10 metrics which outperformed the RAP−index during drainage treatment. A total of 387 drainage events were analyzed in TBI survivors, compared to 298 events in TBI-non survivors. Notably, the number of drainage events in patient 7 and 8 was limited, resulting in less analyzed data of TBI non-survivors compared to TBI survivors. Additionally, accurate measuring drained volumes was only performed in patient 9. Therefore, the results of all metrics in this study need to be validated in a larger and better-balanced patient cohort.

Furthermore, the Python script should be checked for potential errors made in analyzing the ICP signal and obtaining the metrics. Perhaps the script could be improved, e.g. regarding the peak detection of the ICP pulses. This is a limitation, due to two reasons. Firstly, a close inspection

of the ICP pulses often resulted in the presence of e.g. a fourth prevalent peak in the pulse. The clinical significance of the presence of this fourth peak is uncertain. Hence, it may potentially alter the understanding of the ICP pulse waveform. The second reason for this limitation, are the cases where the peaks within the ICP pulse are merged (see figure 2 D and E). Due to the uncertainty of the precise location of the peaks in a merged ICP pulse, this may have resulted in the incorrect identification of peaks as the first, second, or third. Therefore, the obtained results from such pulses could be inaccurate. Nevertheless, since the script is used consistently across all patients, the results remain interpretable and comparable.

Regarding the HFC-power metric, a minor error occurred. Instead of squaring the amplitude A_k in both the numerator and denominator, this was not done in the denominator due to a coding oversight. This results in a metric which is difficult to interpret. However, since this metric showed observable differences in mortality, further investigation into this measure could be worthwhile. In addition, the discussed metrics presented in the results of this study were chosen by a visual inspection. There could be other metrics which also show differences, but were not noticed. The limited number of patients in this study also provides a limitation regarding the results presented in this study. The results give insight into the changes of these metrics over time as well as over drainage in TBI patients, but these insights should be checked in a study with a larger dataset. Another limitation is the identification of a drainage moment. The author of this study manually searched around the nurses timestamp to find the drainage moment, which could have caused wrong identification of drainage moments. Nevertheless, most of the drainage events showed a similar shape, characterized by a relative sharp decline in the ICP, which made them identifiable.

With respect to the viscoelastic model, a possible mistake could have been made in deriving the differential equations as well as the translation into a state space system. The derived state-space representation should be checked and verified before further exploration of the added value of this model, as well as improvement such as the parameter optimization, in a clinical setting is possible.

6.4 Future research

A first objective for further research would be to check whether the observed differences in metrics in this study are also observed in a larger dataset. Regarding the results over time, the choice for a five-period moving average in this study was based on future clinical implementation. This means that when a certain metric, which showed a difference in mortality such as the dP2/dP1 ratio, is implemented in clinical practice on the ICU, the trend of this ratio could be followed at the bedside using the last five drainage moments. This would made implementation of these metrics relative simple and could give the clinical physicians new insights at the bedside of the patient.

Regarding the annotation of the drained volume during a drainage event, the recommendation would be to exactly annotate the drained volume. If this information is present, the ICC can be directly calculated with the pressure drop of the drainage event as was done in patient 9. The value for the ICC can then be compared to e.g. the analyzed metrics in this study and/or with the viscoelastic model, in order to verify the accuracy of accessing the ICC with these metrics. Even without the additional analyzed metrics, accurately measuring drained volumes could provide clinical physicians immediate insights into the ICC of a TBI patient.

Furthermore, peak detection in ICP pulses with merged peaks morphologies should be investigated thoroughly. These peaks may not have been identified in this study due to their low curvature value. Therefore, future research could focus on analyzing ICP pulses with merged peaks to improve peak detection and explore the potential additional information which these ICP pulses with merged peaks contain.

Before a feasible clinical implementation is possible for the viscoelastic model, further development and validation across a larger patient cohort are necessary. The primary focus of this development should be to improve the parameter optimization, enabling the model to simulate an ICP pulse which closely resembles the measured ICP pulse of a TBI patient.

6.5 Conclusion

The results of 10 analyzed metrics in this study are clinically relevant and outperform the RAP−index in accessing the ICC as well as differentiating the mortality of TBI patients on the ICU. The second−to−first peak ratio (dP2/dP1 ratio) shows notable differences in TBI mortality at the start of a drainage treatment. The third−to−second peak ratio (dP3/dP2 ratio) as well as the curvature of the first peak (Curv1) both show immediate observable effects after a single drainage event. The dP2/dP1 ratio, dP3/dP2 ratio and Curv1 thus provide the highest predictive power in assessing the ICC and mortality at the bedside of TBI patients. Advancements in ICP pulse morphology and ICC analysis could enable an implementation of bedside monitoring of these metrics, providing crucial insights for clinical physicians in accessing the ICC of TBI patients based on ICP pulse morphology.

7 Bibliography

1. Instituut FN. Schokkende cijfers over hersenaandoeningen. Accessed on 30th June 2023. Available from: https://www.fninstitute.com/nl/nieuws/schokkende-cijfers-over-hersenaandoeningen
2. Denchev K, Gomez J, Chen P, and Rosenblatt K. Traumatic brain injury: intraoperative management and intensive care unit multimodality monitoring. Anesthesiology clinics 2023; 41:39–78
3. Wilson MH. Monro-Kellie 2.0: The dynamic vascular and venous pathophysiological components of intracranial pressure. Journal of Cerebral Blood Flow & Metabolism 2016; 36:1338–50
4. Benson J, Madhavan A, Cutsforth-Gregory J, Johnson D, and Carr C. The Monro-Kellie Doctrine: A Review and Call for Revision. American Journal of Neuroradiology 2023; 44:2–6
5. Freeman WD. Management of intracranial pressure. CONTINUUM: Lifelong Learning in Neurology 2015; 21:1299–323
6. Harary M, Dolmans R, and Gormley W. Intracranial Pressure Monitoring—Review and Avenues for Development. Sensors 2018 Feb; 18:465. DOI: 10.3390/s18020465
7. Hu X, Xu P, Asgari S, Vespa P, and Bergsneider M. Forecasting ICP elevation based on prescient changes of intracranial pressure waveform morphology. IEEE Transactions on Biomedical Engineering 2010; 57:1070–8
8. Carney N, Totten AM, O'Reilly C, Ullman JS, Hawryluk GW, Bell MJ, Bratton SL, Chesnut R, Harris OA, Kissoon N, et al. Guidelines for the management of severe traumatic brain injury. Neurosurgery 2017; 80:6–15
9. Helbok R, Meyfroidt G, and Beer R. Intracranial pressure thresholds in severe traumatic brain injury: Con: The injured brain is not aware of ICP thresholds! Intensive care medicine 2018; 44:1318–20
10. Mount C and Das J. Cerebral Perfusion Pressure. StatPearls [Internet] 2023. Available from: https://www.ncbi.nlm.nih.gov/books/NBK537271/
11. Nucci CG, De Bonis P, Mangiola A, Santini P, Sciandrone M, Risi A, and Anile C. Intracranial pressure wave morphological classification: automated analysis and clinical validation. Acta neurochirurgica 2016; 158:581–8
12. Kazimierska A, Manet R, Vallet A, Schmidt E, Czosnyka Z, Czosnyka M, and Kasprowicz M. Analysis of intracranial pressure pulse waveform in studies on cerebrospinal compliance: a narrative review. Physiological Measurement 2023
13. Calviello L, Donnelly J, Cardim D, Robba C, Zeiler F, Smielewski P, and Czosnyka M. Compensatory-reserve-weighted intracranial pressure and its association with outcome after traumatic brain injury. Neurocritical care 2018; 28:212–20
14. Zeiler FA, Ercole A, Cabeleira M, Beqiri E, Zoerle T, Carbonara M, Stocchetti N, Menon DK, Smielewski P, Czosnyka M, et al. Compensatory-reserve-weighted intracranial pressure versus intracranial pressure for outcome association in adult traumatic brain injury: a CENTER-TBI validation study. Acta neurochirurgica 2019; 161:1275–84
15. Czosnyka M and Pickard JD. Monitoring and interpretation of intracranial pressure. Journal of Neurology, Neurosurgery & Psychiatry 2004; 75:813–21

16. Varsos GV, Kasprowicz M, Smielewski P, and Czosnyka M. Model-based indices describing cerebrovascular dynamics. Neurocritical care 2014; 20:142–57

17. Eide PK, Sorteberg A, Meling TR, and Sorteberg W. The effect of baseline pressure errors on an intracranial pressure-derived index: results of a prospective observational study. Biomedical engineering online 2014; 13:1–18

18. Hall A and O'Kane R. The best marker for guiding the clinical management of patients with raised intracranial pressure—the RAP index or the mean pulse amplitude? Acta neurochirurgica 2016; 158:1997–2009

19. Czosnyka M, Steiner L, Balestreri M, Schmidt E, Smielewski P, Hutchinson P, and Pickard J. Concept of "true ICP" in monitoring and prognostication in head trauma. *Intracranial Pressure and Brain Monitoring XII*. Springer. 2005 :341–4

20. Scalzo F, Liebeskind D, and Hu X. Reducing false intracranial pressure alarms using morphological waveform features. IEEE Transactions on biomedical engineering 2012; 60:235–9

21. Hamilton R, Xu P, Asgari S, Kasprowicz M, Vespa P, Bergsneider M, and Hu X. Forecasting intracranial pressure elevation using pulse waveform morphology. *2009 annual international conference of the IEEE engineering in medicine and biology society*. IEEE. 2009 :4331–4

22. Leeuw A de. Intracranial pressure pulse morphology and intracranial compliance analysis during liquor drainage in patients with traumatic brain injury. Technical Medicine Internship Report. 2023

23. Uryga A, Ziółkowski A, Kazimierska A, Pudełko A, Mataczyński C, Lang EW, Czosnyka M, and Kasprowicz M. Analysis of intracranial pressure pulse waveform in traumatic brain injury patients: a CENTER-TBI study. Journal of neurosurgery 2022; 139:201–11

24. Robertson CS, Narayan RK, Contant CF, Grossman RG, Gokaslan ZL, Pahwa R, Caram P, Bray RS, and Sherwood AM. Clinical experience with a continuous monitor of intracranial compliance. Journal of neurosurgery 1989; 71:673–80

25. Bray R, Sherwood A, Halter J, Robertson C, and Grossman R. Development of a clinical monitoring system by means of ICP waveform analysis. *Intracranial Pressure VI: Proceedings of the Sixth International Symposium on Intracranial Pressure Held in Glasgow, Scotland, June 9–13, 1985*. Springer. 1986 :260–4

26. Contant Jr CF, Robertson CS, Crouch J, Gopinath SP, Narayan RK, and Grossman RG. Intracranial pressure waveform indices in transient and refractory intracranial hypertension. Journal of Neuroscience methods 1995; 57:15–25

27. Berdyga J, Czosnyka M, Czernicki Z, and Williamson M. Analysis of the intracranial pressure waveform by means of spectral methods. *Intracranial pressure VIII*. Springer. 1993 :372–5

28. Zakrzewska AP, Placek MM, Czosnyka M, Kasprowicz M, and Lang EW. Intracranial pulse pressure waveform analysis using the higher harmonics centroid. Acta neurochirurgica 2021; 163:3249–58

29. Doron O, Zadka Y, Barnea O, and Rosenthal G. Interactions of brain, blood, and CSF: a novel mathematical model of cerebral edema. Fluids and Barriers of the CNS 2021; 18:1–14

30. Nassir A, Rosenthal G, Zadka Y, Houri S, Doron O, and Barnea O. Estimating intracranial parameters using an inverse mathematical model with viscoelastic elements that closely predicts complex ICP morphologies. Computer Methods in Biomechanics and Biomedical Engineering 2024 :1–13

31. Spiegelberg A, Preuß M, and Kurtcuoglu V. B-waves revisited. Interdisciplinary Neurosurgery 2016; 6:13–7

32. Ocamoto GN, Russo TL, Mendes Zambetta R, Frigieri G, Hayashi CY, Brasil S, Rabelo NN, and Spavieri Júnior DL. Intracranial compliance concepts and assessment: a scoping review. Frontiers in Neurology 2021; 12:756112

33. Godoy DA, Brasil S, Iaccarino C, Paiva W, and Rubiano AM. The intracranial compartmental syndrome: a proposed model for acute brain injury monitoring and management. Critical Care 2023; 27:137

34. Bernard F, Barsan W, Diaz-Arrastia R, Merck LH, Yeatts S, and Shutter LA. Brain Oxygen Optimization in Severe Traumatic Brain Injury (BOOST-3): a multicentre, randomised, blinded-endpoint, comparative effectiveness study of brain tissue oxygen and intracranial pressure monitoring versus intracranial pressure alone. BMJ open 2022; 12:e060188

35. Citerio G, Oddo M, and Taccone FS. Recommendations for the use of multimodal monitoring in the neurointensive care unit. Current opinion in critical care 2015; 21:113–9

36. Spyder version 5.5.1. Accessed on 25th March 2024. Available from: `https://www.spyder-ide.org/`

37. Hu X, Xu P, Scalzo F, Vespa P, and Bergsneider M. Morphological clustering and analysis of continuous intracranial pressure. IEEE Transactions on Biomedical Engineering 2008; 56:696–705

38. Nelder JA and Mead R. A simplex method for function minimization. The computer journal 1965; 7:308–13

39. Byrd RH, Lu P, Nocedal J, and Zhu C. A limited memory algorithm for bound constrained optimization. SIAM Journal on scientific computing 1995; 16:1190–208

40. Ravichandran S, Manoharan P, Sinha DK, Jangir P, Abualigah L, and Alghamdi TA. Multi-objective resistance-capacitance optimization algorithm: An effective multi-objective algorithm for engineering design problems. Heliyon 2024; 10

8 Appendices

A: Figures

In this appendix supplementary figures are shown.

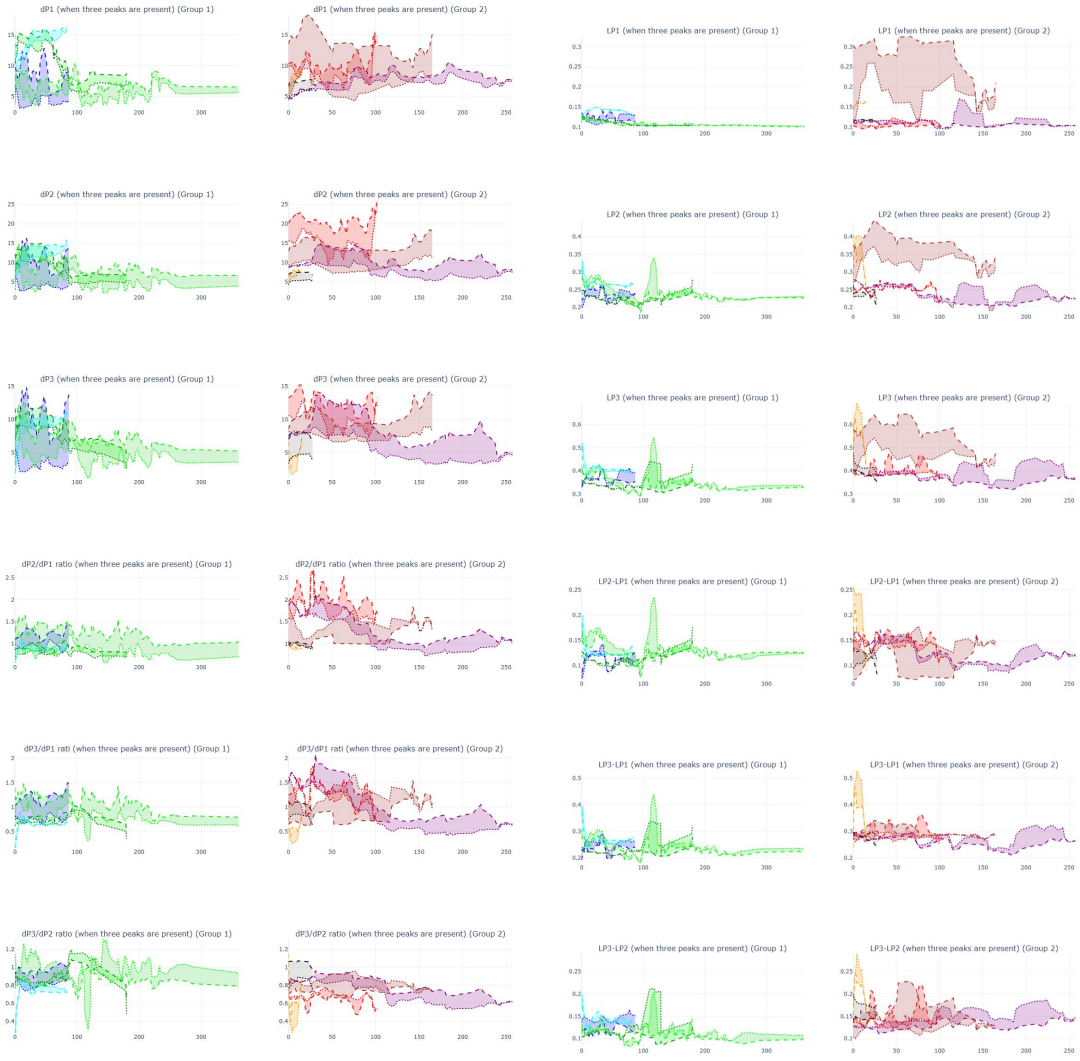

Figure 22: *Several metrics shown over time, with the metric on the y-axis and absolute time after the first drainage event in hours on the x-axis. Data of TBI survivors, patient 1-4, is shown on the left panel as 'Group 1' and is indicated in blue, green, cyan and lime, respectively. Data of TBI non-survivors, patient 5-9, is shown on the right panel as 'Group 2' and is indicated in red, purple, orange, black and brown, respectively. The data is presented as a 5-period moving average to enhance visibility and facilitate the identification of potential trends over time. The dashed line represents the values before drainage, the dotted line represents values after drainage. The area between these lines is shaded for each patient to enhance visibility and quantify the extent of change over a single drainage event. TBI: Traumatic Brain Injury.*

Figure 23: *Several metrics shown over time, with the metric on the y-axis and absolute time after the first drainage event in hours on the x-axis. Data of TBI survivors, patient 1-4, is shown on the left panel as 'Group 1' and is indicated in blue, green, cyan and lime, respectively. Data of TBI non-survivors, patient 5-9, is shown on the right panel as 'Group 2' and is indicated in red, purple, orange, black and brown, respectively. The data is presented as a 5-period moving average to enhance visibility and facilitate the identification of potential trends over time. The dashed line represents the values before drainage, the dotted line represents values after drainage. The area between these lines is shaded for each patient to enhance visibility and quantify the extent of change over a single drainage event. TBI: Traumatic Brain Injury.*

Figure 24: *Several metrics shown over time, with the metric on the y-axis and absolute time after the first drainage event in hours on the x-axis. Data of TBI survivors, patient 1-4, is shown on the left panel as 'Group 1' and is indicated in blue, green, cyan and lime, respectively. Data of TBI non-survivors, patient 5-9, is shown on the right panel as 'Group 2' and is indicated in red, purple, orange, black and brown, respectively. The data is presented as a 5-period moving average to enhance visibility and facilitate the identification of potential trends over time. The dashed line represents the values before drainage, the dotted line represents values after drainage. The area between these lines is shaded for each patient to enhance visibility and quantify the extent of change over a single drainage event. TBI: Traumatic Brain Injury.*

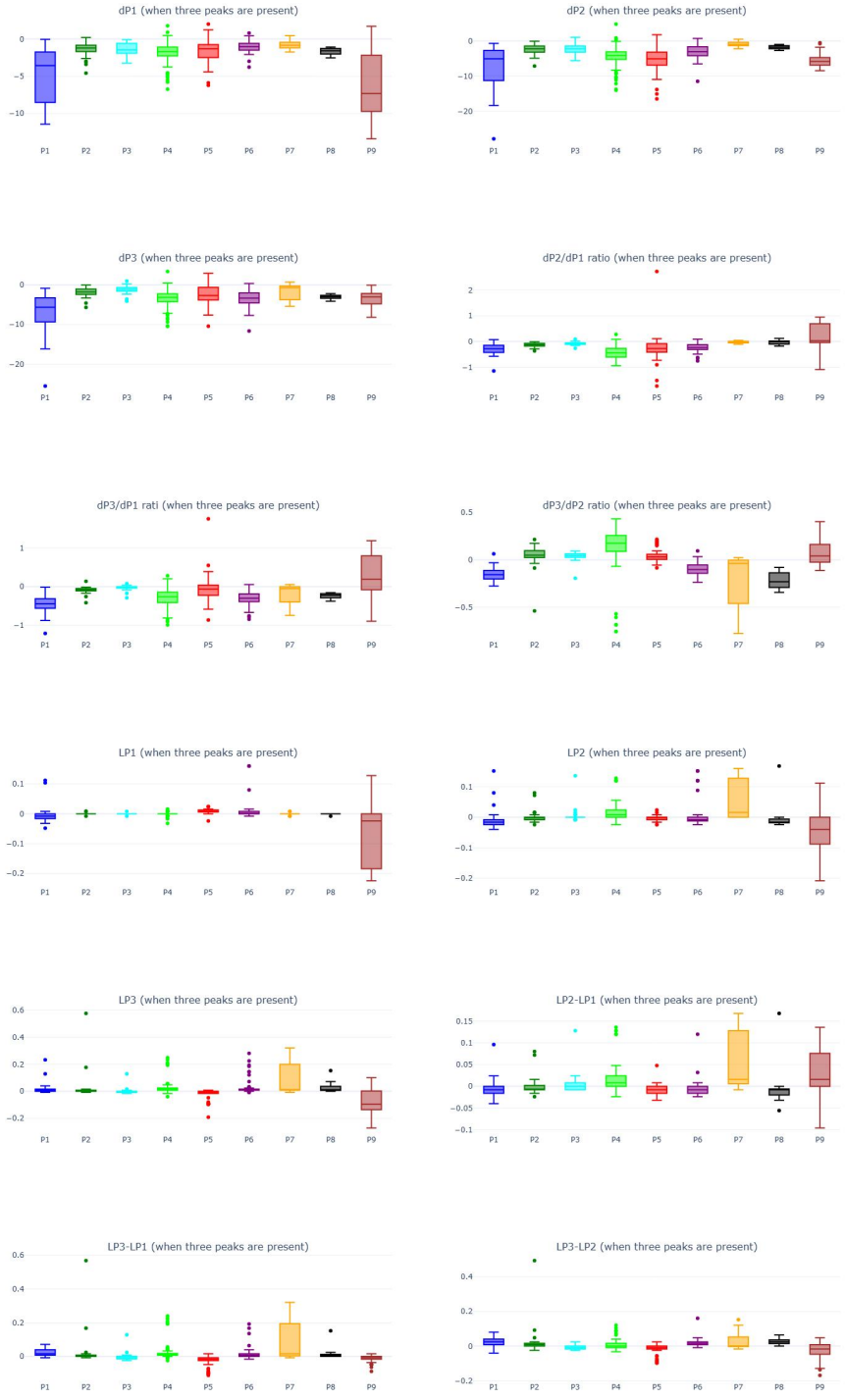

Figure 25: *Change in several metrics over a single drainage event is shown for each patient, indicated by P1-P9. Data of TBI survivors, patient 1-4, is indicated in blue, green, cyan and lime, respectively. Data of TBI non-survivors, patient 5-9, is indicated in red, purple, orange, black and brown, respectively. The data is presented as a boxplot. The edges of the boxes indicate the 25th (Q1) and 75th (Q3) percentiles, whereas whiskers give the minimum and maximum values. Outliers are presented as single dots outside these whiskers. TBI: Traumatic Brain Injury.*

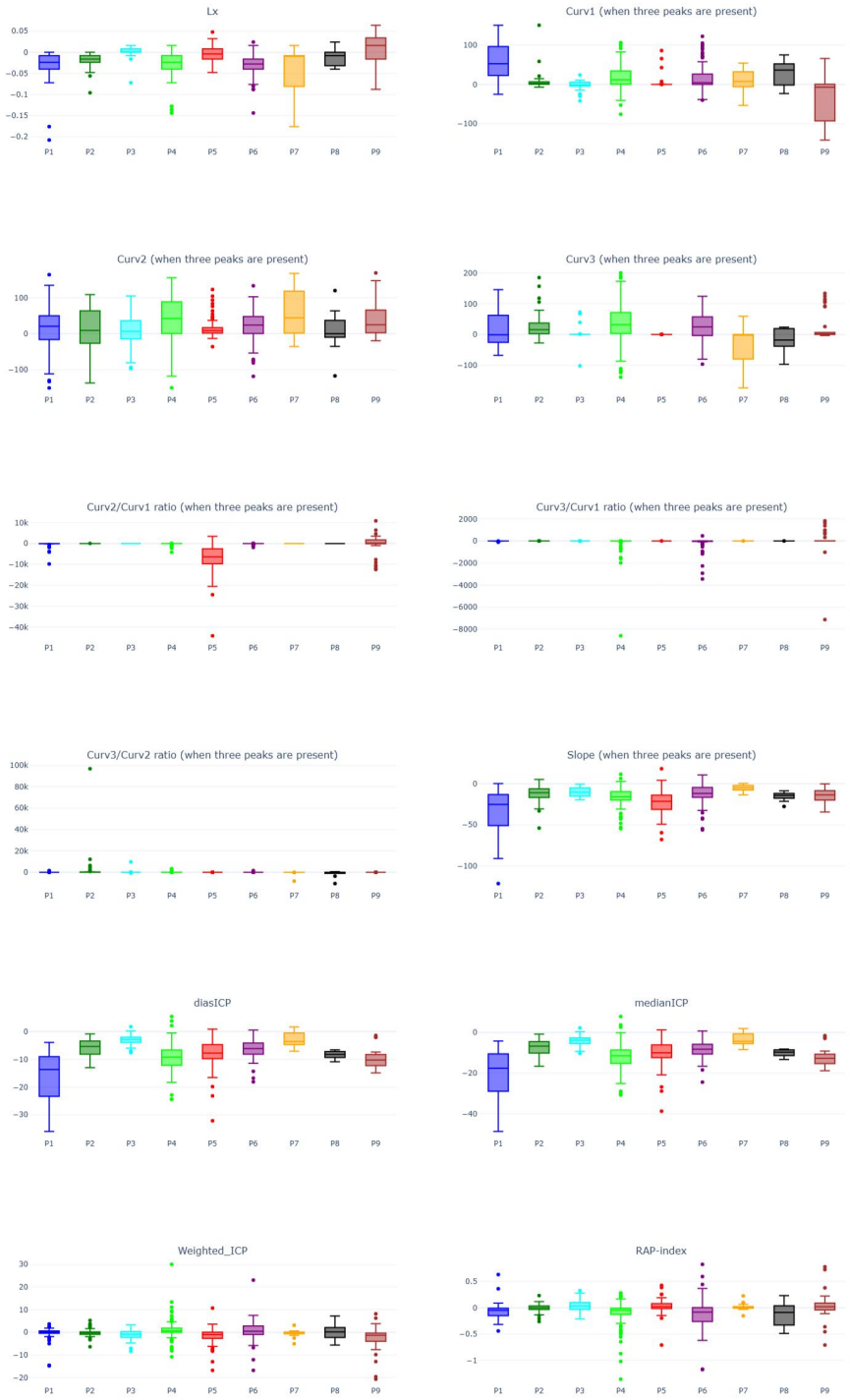

Figure 26: *Change in several metrics over a single drainage event is shown for each patient, indicated by P1-P9. Data of TBI survivors, patient 1-4, is indicated in blue, green, cyan and lime, respectively. Data of TBI non-survivors, patient 5-9, is indicated in red, purple, orange, black and brown, respectively. The data is presented as a boxplot. The edges of the boxes indicate the 25th (Q1) and 75th (Q3) percentiles, whereas whiskers give the minimum and maximum values. Outliers are presented as single dots outside these whiskers. TBI: Traumatic Brain Injury.*

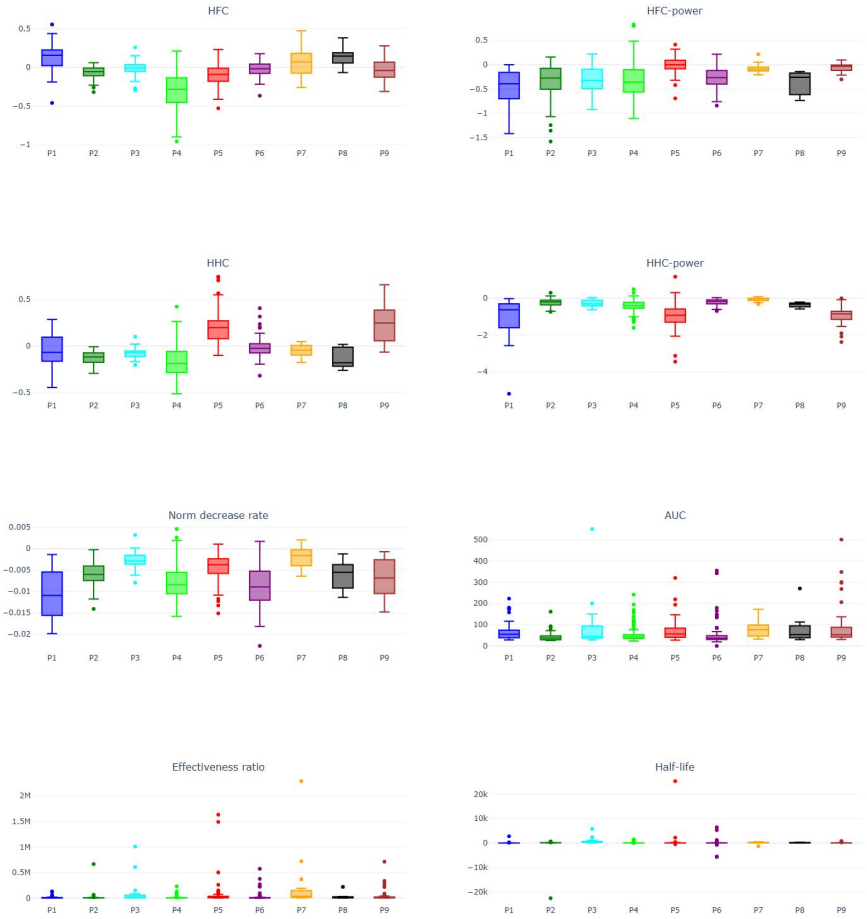

Figure 27: *Change in several metrics over a single drainage event is shown for each patient, indicated by P1-P9. Data of TBI survivors, patient 1-4, is indicated in blue, green, cyan and lime, respectively. Data of TBI non-survivors, patient 5-9, is indicated in red, purple, orange, black and brown, respectively. The data is presented as a boxplot. The edges of the boxes indicate the 25th (Q1) and 75th (Q3) percentiles, whereas whiskers give the minimum and maximum values. Outliers are presented as single dots outside these whiskers. TBI: Traumatic Brain Injury.*

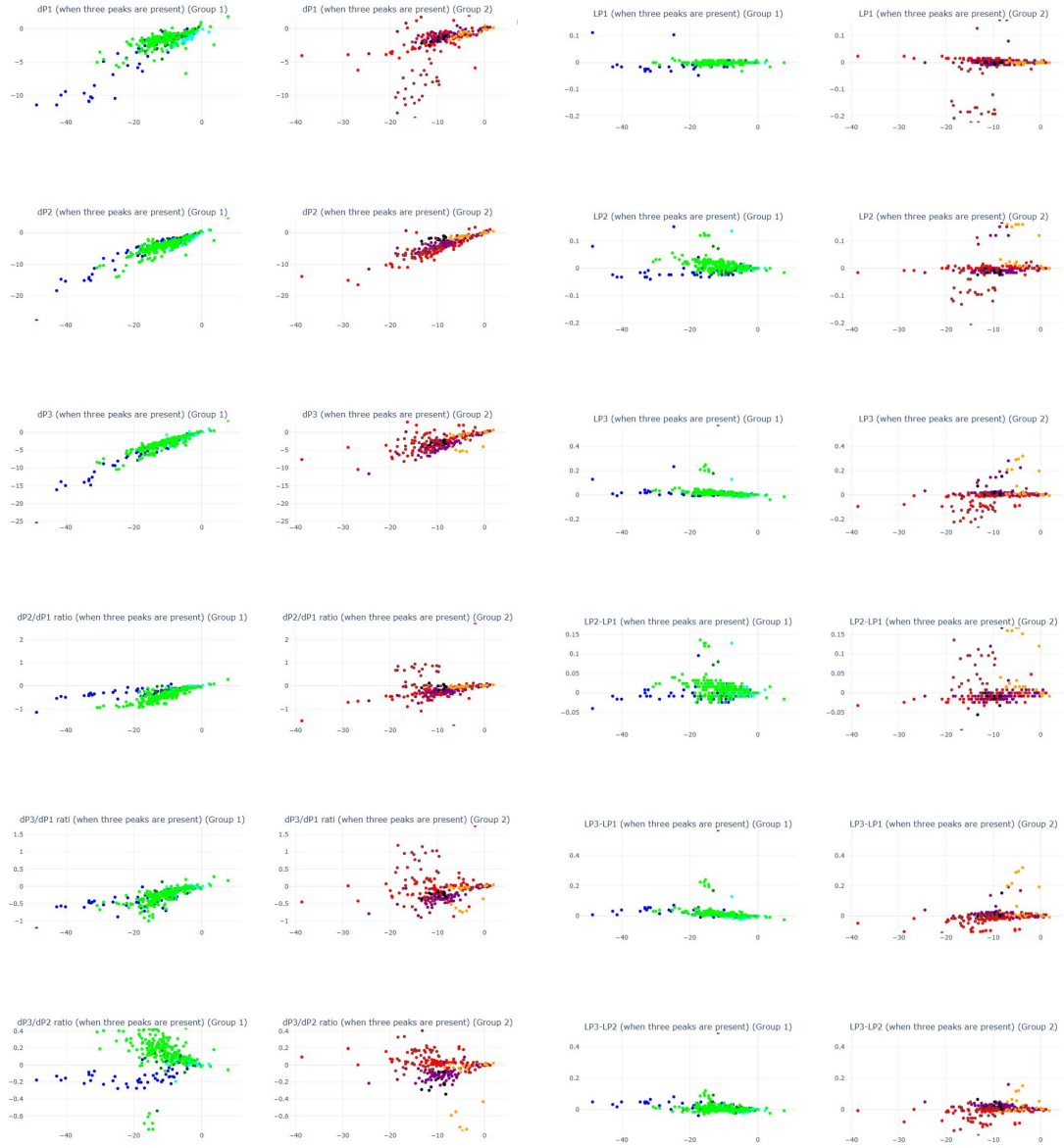

Figure 28: *Change of several metrics is shown on the y-axis with the accompanying change in ICP in mmHg on the x-axis over a single drainage event. Data of TBI survivors, patient 1-4, is shown on the left panel as 'Group 1' and is indicated in blue, green, cyan and lime, respectively. Data of TBI non-survivors, patient 5-9, is shown on the right panel as 'Group 2' and is indicated in red, purple, orange, black and brown, respectively. ICP: Intracranial Pressure, TBI: Traumatic Brain Injury.*

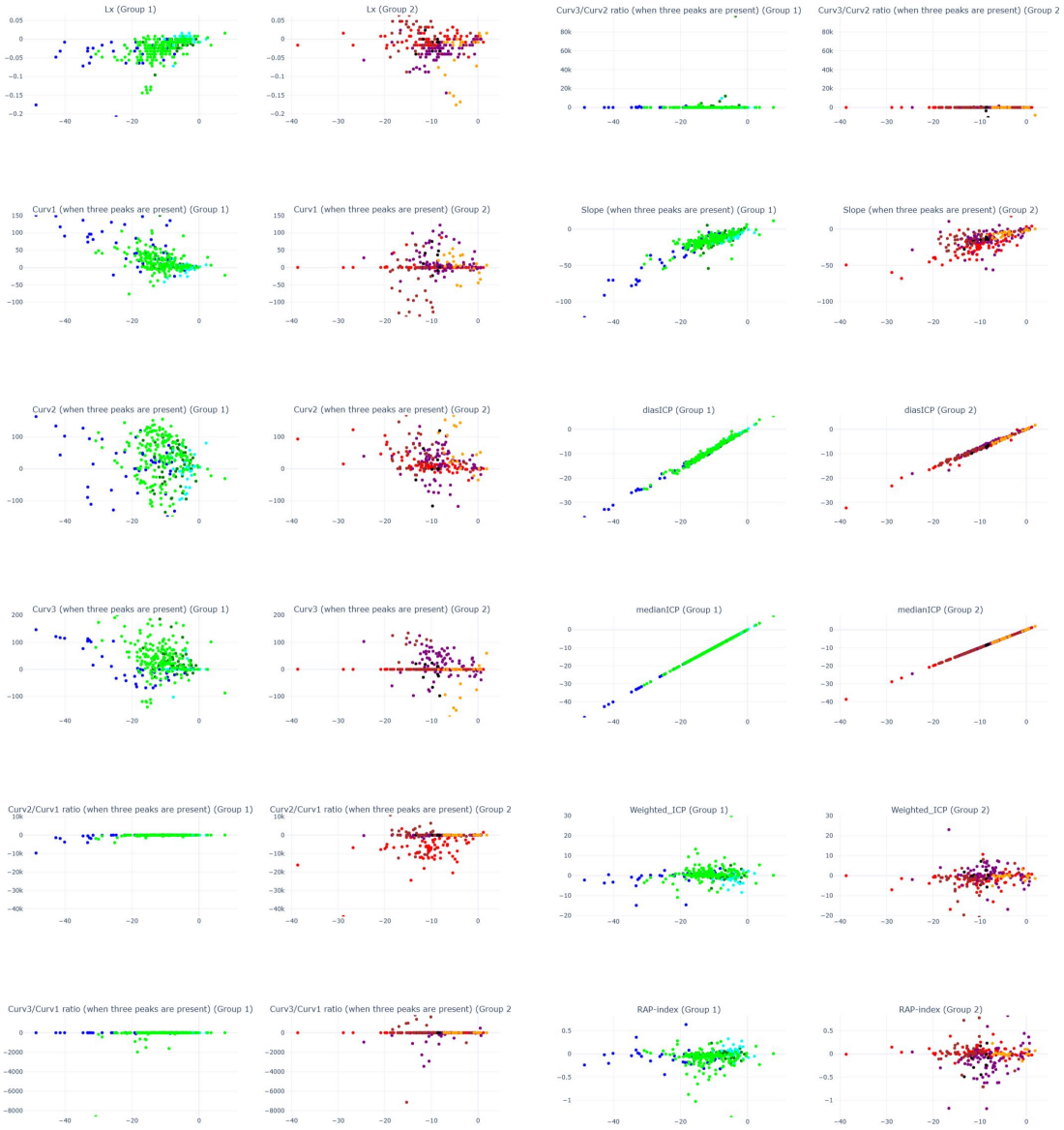

Figure 29: *Change of several metrics is shown on the y-axis with the accompanying change in ICP in mmHg on the x-axis over a single drainage event. Data of TBI survivors, patient 1-4, is shown on the left panel as 'Group 1' and is indicated in blue, green, cyan and lime, respectively. Data of TBI non-survivors, patient 5-9, is shown on the right panel as 'Group 2' and is indicated in red, purple, orange, black and brown, respectively. ICP: Intracranial Pressure, TBI: Traumatic Brain Injury.*

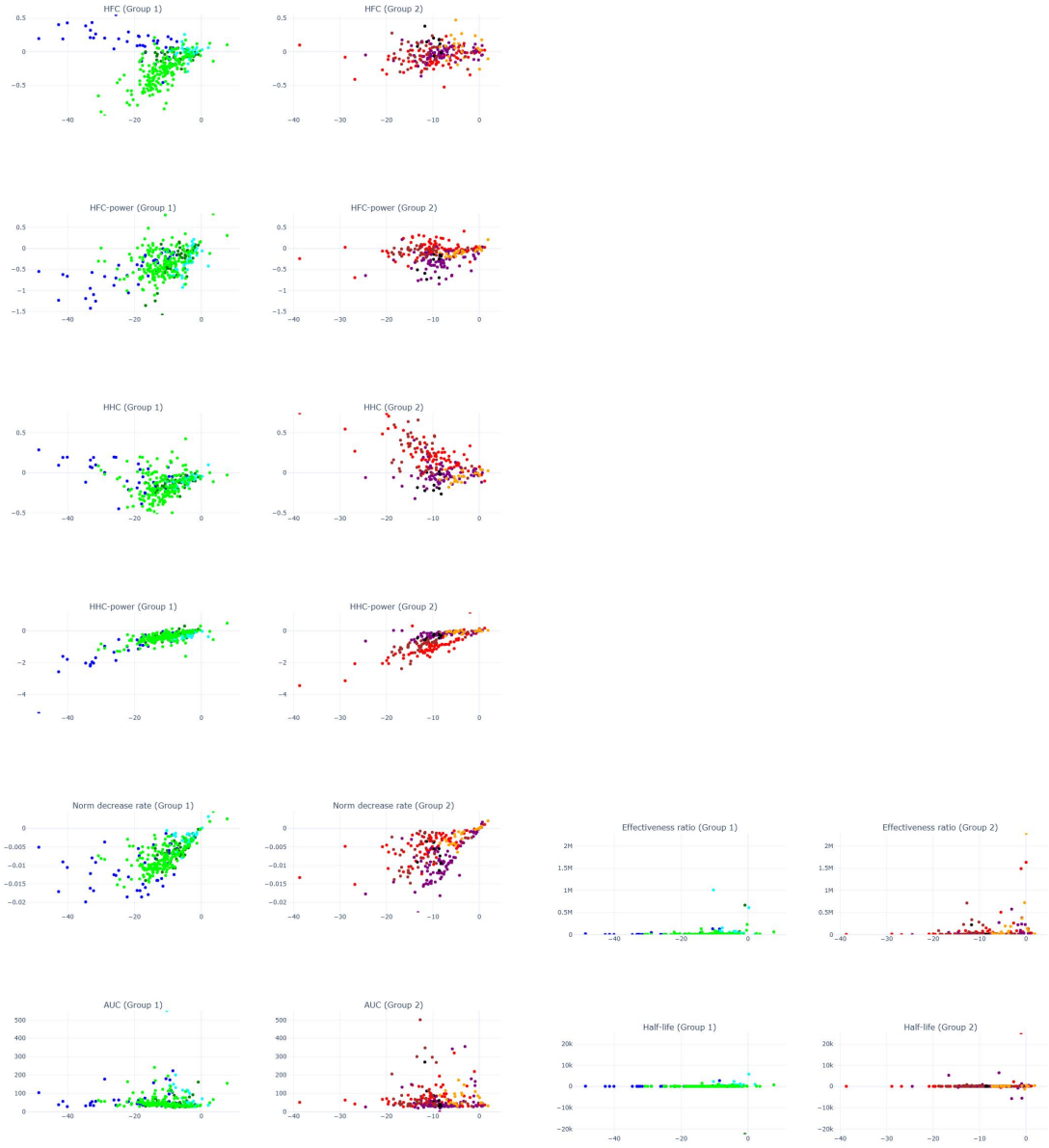

Figure 30: *Change of several metrics is shown on the y-axis with the accompanying change in ICP in mmHg on the x-axis over a single drainage event. Data of TBI survivors, patient 1-4, is shown on the left panel as 'Group 1' and is indicated in blue, green, cyan and lime, respectively. Data of TBI non-survivors, patient 5-9, is shown on the right panel as 'Group 2' and is indicated in red, purple, orange, black and brown, respectively. ICP: Intracranial Pressure, TBI: Traumatic Brain Injury.*

B: Viscoelastic model

The results of the obtained state-space model matrices can be found on the next page. The used abbreviations for the resistances and compliances can be found in figure 7 on page 17. Due to the large number of parameters, several new parameters were introduced to enhance clarity and visibility. These new parameters thus represent combinations of multiple original parameters:

$$A_{\text{mod}} = \frac{RV \cdot RCA}{(RCV \cdot CV) \cdot (RC \cdot RA + RC \cdot RCA + RCA \cdot RA)}$$

$$B_{\text{mod}} = \frac{RA}{RC} \cdot A_{\text{mod}}$$

$$D_{\text{mod}} = \frac{RBV}{CV \cdot (RCV \cdot RBV + RV \cdot RBV + RCV \cdot RV)}$$

$$E_{\text{mod}} = \frac{RV}{CV \cdot (RCV \cdot RBV + RV \cdot RBV + RCV \cdot RV)}$$

$$F_{\text{mod}} = \frac{RBV \cdot RCC \cdot CC}{CV \cdot (RCV \cdot RBV + RV \cdot RBV + RCV \cdot RV)}$$

$$G_{\text{mod}} = \frac{RC \cdot RBBB + RC \cdot RV + RBBB \cdot RV}{RC \cdot RBBB \cdot RCV \cdot CV} - B_{\text{mod}}$$

$$H_{\text{mod}} = \frac{RV}{RC \cdot RCV \cdot CV} + B_{\text{mod}} + A_{\text{mod}}$$

$$I_{\text{mod}} = \frac{CC \cdot (RC \cdot RBBB + RC \cdot RCC \cdot RV + RBBB \cdot RCC \cdot RV + RC \cdot RBBB \cdot RCC)}{RC \cdot RBBB \cdot RCV \cdot CV} - RCC \cdot CC \cdot B_{\text{mod}}$$

$$Z_{\text{mod}} = \frac{RC}{CA \cdot (RC \cdot RA + RC \cdot RCA + RCA \cdot RA)}$$

$$X_{\text{mod}} = \frac{RA}{CA \cdot (RC \cdot RA + RC \cdot RCA + RCA \cdot RA)}$$

$$\dot{x}(t) = Ax(t) + Bu(t)$$
$$y(t) = Cx(t) + Du(t)$$

$$A = \begin{bmatrix} -\frac{1}{RCVEN \cdot CVEN} & 0 & 0 & 0 & 0 & 0 & 0 \\ -\frac{RVEN}{RCVEN \cdot RFM \cdot CSPI} & -\frac{1}{RFM \cdot CSPI} & 0 & 0 & 0 & 0 & 0 \\ -\frac{RVEN}{RCVEN \cdot RCSAS \cdot CSAS} & 0 & -\frac{1}{RCSAS \cdot CSAS} & 0 & 0 & 0 & 0 \\ \frac{RVEN}{RCVEN \cdot RCBR \cdot CBR} & 0 & 0 & -\frac{1}{RCBR \cdot CBR} & 0 & 0 & 0 \\ 0 & 0 & 0 & 0 & -(X_{\text{mod}} + Z_{\text{mod}} + \frac{RCC \cdot CC \cdot X_{\text{mod}} \cdot H_{\text{mod}}}{F_{\text{mod}} - I_{\text{mod}}}) & -(X_{\text{mod}} + \frac{RCC \cdot CC \cdot X_{\text{mod}} \cdot (G_{\text{mod}} - D_{\text{mod}})}{F_{\text{mod}} - I_{\text{mod}}}) & -RCC \cdot CC \cdot X_{\text{mod}} \cdot \frac{1}{RCV \cdot CV} + E_{\text{mod}} + D_{\text{mo} \\ 0 & 0 & 0 & 0 & \frac{H_{\text{mod}}}{F_{\text{mod}} - I_{\text{mod}}} & \frac{G_{\text{mod}} - D_{\text{mod}}}{F_{\text{mod}} - I_{\text{mod}}} & \frac{1}{RCV \cdot CV} + E_{\text{mod}} + D_{\text{mod}} \\ 0 & 0 & 0 & 0 & \frac{F_{\text{mod}} \cdot H_{\text{mod}}}{F_{\text{mod}} - I_{\text{mod}}} & \frac{F_{\text{mod}} \cdot G_{\text{mod}} - F_{\text{mod}} \cdot D_{\text{mod}}}{F_{\text{mod}} - I_{\text{mod}}} + D_{\text{mod}} & F_{\text{mod}} \cdot \frac{1}{RCV \cdot CV} + F_{\text{mod}} \cdot E_{\text{mod}} - F_{\text{mod}} \cdot D_{\text{mod}} - E_{\text{mod}} \end{bmatrix}$$

$$B = \begin{bmatrix} 0 & 0 & 0 & 0 \\ 0 & 0 & 0 & -\frac{RVEN}{RFM \cdot CSPI} \\ 0 & 0 & 0 & -\frac{RVEN}{RCSAS \cdot CSAS} \\ 0 & 0 & 0 & \frac{RVEN}{RCBR \cdot CBR} \\ Z_{\text{mod}} - \frac{RCC \cdot CC \cdot X_{\text{mod}} \cdot E_{\text{mod}}}{F_{\text{mod}} - I_{\text{mod}}} & 0 & 0 & 0 \\ \frac{A_{\text{mod}}}{F_{\text{mod}} - I_{\text{mod}}} & \frac{E_{\text{mod}}}{F_{\text{mod}} - I_{\text{mod}}} & 0 & 0 \\ \frac{F_{\text{mod}} \cdot A_{\text{mod}}}{F_{\text{mod}} - I_{\text{mod}}} & \frac{F_{\text{mod}} \cdot E_{\text{mod}}}{F_{\text{mod}} - I_{\text{mod}}} - E_{\text{mod}} & 0 & 0 \end{bmatrix}$$

$$C = \left[-\frac{RBF}{RCVEN} \quad -\frac{RVEN \cdot RBF}{RCVEN \cdot RCBR} \quad -\frac{RVEN}{RCVEN} \quad 0 \quad 0 \quad \frac{RBF}{RCBR} \quad -\frac{RBF \cdot CC \cdot H_{\text{mod}} + RBF \cdot CV \cdot F_{\text{mod}} \cdot H_{\text{mod}} + RBF \cdot CA \cdot RCC \cdot CC \cdot X_{\text{mod}} \cdot H_{\text{mod}}}{F_{\text{mod}} - I_{\text{mod}}} - RBF \cdot CA \cdot (X_{\text{mod}} + Z_{\text{mod}}) \quad -\frac{RBF \cdot CC \cdot (G_{\text{mod}} - D_{\text{mod}}) + RBF \cdot CV \cdot (F_{\text{mod}} \cdot G_{\text{mod}} - F_{\text{mod}} \cdot D_{\text{mod}}) + RBF \cdot CA \cdot RCC \cdot CC \cdot X_{\text{mod}} \cdot (G_{\text{mod}} - D_{\text{mod}})}{F_{\text{mod}} - I_{\text{mod}}} - RBF \cdot CV \cdot D_{\text{mod}} - RBF \cdot CA \cdot X_{\text{mod}} - \frac{RBF}{RBRB} \quad -\frac{RBF \cdot CC \cdot \left(\frac{1}{RCV \cdot CV} + E_{\text{mod}} + D_{\text{mod}} \right) + RBF \cdot CV \cdot \left(\frac{F_{\text{mod}}}{RCV \cdot CV} + F_{\text{mod}} \cdot E_{\text{mod}} - F_{\text{mod}} \cdot D_{\text{mod}} \right) + RBF \cdot CA \cdot RCC \cdot CC \cdot X_{\text{mod}} \cdot \left(\frac{1}{RCV \cdot CV} + E_{\text{mod}} + D_{\text{mod}} \right)}{F_{\text{mod}} - I_{\text{mod}}} - RBF \cdot CV \cdot (-E_{\text{mod}} - D_{\text{mod}}) \right]$$

$$D = \left[-\frac{RBF \cdot CC \cdot A_{\text{mod}} + RBF \cdot CV \cdot F_{\text{mod}} \cdot A_{\text{mod}} + RBF \cdot CA \cdot RCC \cdot CC \cdot X_{\text{mod}} \cdot A_{\text{mod}}}{F_{\text{mod}} - I_{\text{mod}}} + RBF \cdot CA \cdot Z_{\text{mod}} \quad -\frac{RBF \cdot CC \cdot E_{\text{mod}} + RBF \cdot CV \cdot F_{\text{mod}} \cdot E_{\text{mod}} + RBF \cdot CA \cdot RCC \cdot CC \cdot X_{\text{mod}} \cdot E_{\text{mod}}}{F_{\text{mod}} - I_{\text{mod}}} + RBF \cdot CV \cdot E_{\text{mod}} \quad RBF \quad -RVEN - \frac{RVEN \cdot RBF}{RCBR} \right]$$